FCTUC FACULDADE DE CIÊNCIAS
E TECNOLOGIA
UNIVERSIDADE DE COIMBRA

Felipe Vieira Trenk

Evaluation of lung ventilation of COPD patients using EIT

Dissertation submitted to the University of Coimbra to fulfill the requirements for the degree of Master of Science in Engineering Physics program

Supervisors:

Prof. Dr. César Alexandre Domingues Teixeira

Prof. Dr. Paulo Fernando Pereira de Carvalho

Coimbra, 2016

This thesis was developed in collaboration with:

Centro de Informática e Sistemas da Universidade de Coimbra

WELCOME - Wearable Sensing and Smart Cloud Computing for Integrated Care to COPD Patients with Comorbidities

"And once the storm is over you won't remember how you made it through, how you managed to survive. You won't even be sure, in fact, whether the storm is really over. But one thing is certain. When you come out of the storm you won't be the same person who walked in. That's what this storm's all about."

Haruki Murakami, Kafka on the Shore

Aos meus pais

Acknowledgements

First of all, I would like to acknowledge CISUC, the WELCOME project, and the coordinator of the WELCOME project at CISUC, Prof. Dr. Rui Paiva, for providing the conditions required for the realization of this study. I would also like to acknowledge the people that collected the data studied in this work: Prof. Dr. Inéz Frerichs, Dr. Luís Mendes, and the whole medical team led by Prof. Dr. N. Maglavera, Prof. Dr. I. Chouvarda and Dr. V. Tsara. Without them this study would not be possible.

I am especially grateful to have worked with Prof. Dr. César Teixeira from the Department of Informatics Engineering, who is the main supervisor of this work. His support, guidance and expertise were a vital help in overcoming all those unpreventable obstacles that appear with a work of this magnitude. I am also thankful to Prof. Dr. Paulo de Carvalho for providing a sharp analysis and feedback and offer new ideas whenever needed.

My deepest thanks to Dr. Luís Mendes, for going above and beyond helping me with many of the intricacies around EIT medical imaging and being constantly available to answer my many questions. I will always remember his kindness and support in the hardest moments of this year.

I would like to thank my colleagues which made me company during the many, many hours of research and writing, making things much easier to me.

A special thank you to Sara for being such a bright spark in the last 5 years of my life and for always offering a helping hand or a calming voice whenever I needed.

None of my accomplishments would make sense without the presence of my family in my life. I would not be the person I am today without them.

At last, but not least, I am extremely grateful for meeting and keeping so many wonderful friends during this 5-year adventure. My sincerest thanks to all for making these years so enjoyable.

Abstract

Chronic obstructive pulmonary disease (COPD) is widespread worldwide and has a large impact in the patients' quality of life and in global healthcare costs. While an early diagnosis is fundamental to its treatment, it still relies heavily in the patients' medical history and symptomatic spirometry. Parameters based on minimally invasive medical devices able to identify and monitor COPD would be a valuable diagnostic tool to reduce the impact of the disease.

Electrical Impedance Tomography (EIT) is a minimally invasive medical imaging technique that is growing in terms of research, clinical use and global exposure. One of its most promising applications is in monitoring of lung ventilation. This thesis contribution consists on the formulation or adaptation, implementation and testing of three different parameters that measure lung ventilation heterogeneity: the Global Inhomogeneity (GI) index, the Local Inhomogeneity (LI) index and the Percentage of Pixels (PoP) index. The long term objective is the use of one or several of these parameters, depending on the results of this study, in identification and monitoring of COPD patients.

Datasets of two groups were acquired during tidal breathing: a group of patients with COPD and a control group. A selection of these datasets was made after an evaluation of the amplitude of each breathing cycle and the overall noise of the acquisition. Images were reconstructed using the Graz consensus Reconstruction algorithm for Electrical Impedance Tomography (GREIT) and an adult thorax shaped model of the EIDORS library. For each breathing cycle a tidal image was computed. The three parameters were tested on these images.

Performance of the parameters were analysed using the Kruskall-Wallis test and the Receiver Operating Characteristic (ROC) curve. The PoP index exhibited the most promising results from the parameters studied. The Kruskal-Wallis test and cross validation returned significant differences between the control and the COPD group. The ROC curve analysis also demonstrated a strong performance in terms of classification.

Keywords: *Chronic obstructive pulmonary disease, medical imaging, electrical impedance tomography, lung ventilation inhomogeneity*

Resumo

A doença pulmonar obstrutiva crónica (COPD) é uma doença global com um alto impacto na qualidade de vida dos pacientes e em custos de saúde. Uma identificação rápida da doença é crucial para o seu tratamento. Contudo, essa identificação ainda depende principalmente da história médica do paciente e um exame de espirometria. Algoritmos de identificação e monitorização a longo prazo de pacientes com COPD seriam portanto uma ferramenta de diagnóstico valiosa para minimizar o impacto da doença.

Tomografia por impedância eléctrica (EIT) é uma técnica de imagem médica não-invasiva em franco crescimento em termos de pesquisa científica, utilização clínica e exposição global. Uma das suas aplicações mais promissoras encontra-se na monitoração da ventilação pulmonar. Este projecto pretende formular ou adaptar, implementar e testar três parâmetros que calculam a heterogeneidade da ventilação a partir das imagens obtidas por esta técnica: os indíces *Global Inhomogeneity* (GI), *Local Inhomogeneity* (LI) e *Percentage of Pixels* (PoP). O objectivo a longo prazo é a utilização de um ou vários destes parâmetros, dependendo dos resultados obtidos durante este projecto, na identificação e monitorização de pacientes com COPD.

Foram adquiridos dados de dois grupos durante respiração tidal: um grupo de pacientes com a doença mencionada e um grupo de controlo. Imagens foram reconstruídas com o *Graz consensus Reconstruction algorithm for Electrical Impedance Tomography* (GREIT) e utilizando um modelo de um tórax de um adulto disponibilizado pela biblioteca EIDORS. Para cada ciclo de respiração uma imagem tidal foi calculada, a partir da qual os três parâmetros foram calculados.

Um analise estatística foi realizada usando um teste de *Kruskall-Wallis* e a performance da cada parâmetro foi avaliada calculadno a curva da Característica de Operação do Receptor (ROC). Dos parâmetros estudados o índice PoP obteve os resultados mais promissores. Foram obtidas diferenças significativas no teste de *Kruskall-Wallis* e na validação cruzada que se realizaram. A análise à curva ROC demonstra que o parâmetro tem um bom desempenho em termos de classificação.

Palavras-Chave: *Doença pulmonar obstrutiva crónica, imagem médica, tomografia por impedância eléctrica, ventilação pulmonar heterogénea*

Abbreviations

APD	**A**verage **P**ixel **D**ifference
AR	**A**mplitude **R**esponse
ARDS	**A**cute **R**espiratory **D**istress **S**yndrome
AUC	**A**rea **U**nder **C**urve
CoG	**C**entre **o**f **G**ravity
COPD	**C**hronic **O**bstructive **P**ulmonary **D**isease
CT	**C**omputerized **T**omography
EIT	**E**lectrical **I**mpedance **T**omography
FFT	**F**ast **F**ourier **T**ransform
GI	**G**lobal **I**nhomogeneity index
GIC	**G**lobal **I**mpedance **C**urve
GREIT	**G**raz consensus **R**econstruction algorithm for **E**lectrical **I**mpedance **T**omography
LI	**L**ocal **I**nhomogeneity index
LPV	**L**ung **P**rotective **V**entilation
MRI	**M**agnetic **R**esonance **I**maging
PE	**P**osition **E**rror
PSF	**P**oint **S**pread **F**unction
RES	**Res**olution
RNG	**R**i**ng**ing
ROC	**R**eceiver **O**perating **C**haracteristic
ROI	**R**egion **o**f **I**nterest
SD	**S**tandard **D**eviation
SHD	**Sh**ape **D**eformation
VALI	**V**entilator **A**ssociated **L**ung **I**njuries
VILI	**V**entilator **I**nduced **L**ung **I**njuries

WHO **W**orld **H**ealth **O**rganization

YLD **Y**ears **L**ived with **D**isability

List of Figures

1.1 The ten leading causes of death in the world in 2012. 1

2.1 Structure of the lung and alveoli. 5
2.2 Comparison of the top 10 causes of deaths across income groups. 6
2.3 Typical steps for EIT data analysis 8
2.4 Some of the areas of application of EIT. 10
2.5 Data acquisition of an EIT system with 16 electrodes that uses adjacent current stimulation 12

3.1 Adult thorax shaped model selected from the model library. 18
3.2 Global impedance curve obtained of one dataset. 19
3.3 Obtained image after reconstruction at end-inspiration, the following end-expiration and the resulting tidal image. 19
3.4 Global impedance curve obtained for one dataset with an unacceptable amount of noise. 20
3.5 Global impedance curve obtained for one dataset with small impedance differences during acquisitions. 21
3.6 FFT spectrum for the global impedance curve of a dataset with normal noise and a dataset with excessive noise. 22

4.1 Comparison of the GI values for the COPD patients and the control group. 28
4.2 Cross validation of the GI index. 30
4.3 Cross validation of the GI index between the female control group and the female COPD group. 31
4.4 Cross validation of the GI index between the male control group and the male COPD group. 31
4.5 Comparison of the obtained LI values for the COPD patients and the control group. 34
4.6 Cross validation of the LI index. 34
4.7 Comparison of the obtained PoP values for the COPD patients and the control group. 37
4.8 Cross validation of the PoP index. 37
4.9 Cross validation of the PoP index between the female control group and the female COPD group. 38
4.10 Cross validation of the PoP index between the male control group and the male COPD group. 38
4.11 ROC for classification by Logistic Regression. 40

A.1 Performance figures of merit selected for evaluation of GREIT images. . . 50

A.2 Schematic representation of the Noise Figure parameter. 53

B.1 Tidal image obtained from healthy subject #5. 55
B.2 Tidal image obtained from healthy subject #6. 55
B.3 Tidal image obtained from healthy subject #7. 56
B.4 Tidal image obtained from healthy subject #8. 56
B.5 Tidal image obtained from healthy subject #9. 56
B.6 Tidal image obtained from healthy subject #10. 57
B.7 Tidal image obtained from patient #1. 57
B.8 Tidal image obtained from patient #2. 57
B.9 Tidal image obtained from patient #3. 58
B.10 Tidal image obtained from patient #4. 58
B.11 Tidal image obtained from patient #5. 58
B.12 Tidal image obtained from patient #6. 59
B.13 Tidal image obtained from patient #7. 59
B.14 Tidal image obtained from patient #8. 59
B.15 Tidal image obtained from patient #9. 60
B.16 Tidal image obtained from patient #10. 60
B.17 Tidal image obtained from patient #11. 60
B.18 Tidal image obtained from patient #12. 61
B.19 Tidal image obtained from patient #13. 61
B.20 Tidal image obtained from patient #14. 61

List of Tables

2.1 Typical values of tissue resistivity at a frequency of about 10 kHz 8

3.1 Evaluation of the data acquisition quality of healthy subjects. 23
3.2 Evaluation of the data acquisition quality of the COPD patients. 24

4.1 Average GI obtained for each dataset of the control group. 28
4.2 Average GI obtained for each dataset of the COPD group. 29
4.3 Average LI obtained for each dataset of the control group. 32
4.4 Average LI obtained for each dataset of the COPD group. 33
4.5 Average PoP obtained for each dataset of the control group. 35
4.6 Average PoP obtained for each dataset of the COPD group. 36

Contents

Acknowledgements **ix**

Abstract **xi**

Resumo **xiii**

Abbreviations **xv**

List of Figures **xvii**

List of Tables **xix**

Contents **xxii**

1 Introduction **1**
1.1 Problem Contextualization and Motivation 1
1.2 Objectives 3
1.3 Document Overview 3
1.4 Scientific Contributions 4

2 Background concepts on COPD and EIT lung monitoring **5**
2.1 COPD: an overview 5
2.1.1 Impact 6
2.1.2 Risk factors and symptoms 7
2.2 EIT and real time monitoring of pulmonary ventilation 7
2.2.1 The general concept behind medical EIT 7
2.2.2 Applications, opportunities and challenges 8
2.2.2.1 Temporal and spatial resolution 10
2.2.2.2 EIT sensitivity and difference imaging 11
2.3 EIT System Architecture 11
2.4 EIT reconstruction algorithms 13
2.4.1 Linear reconstruction algorithms 14
2.4.2 Graz consensus Reconstruction algorithm for EIT (GREIT) 15

3 Materials and Methods **17**
3.1 Data Acquisition 17
3.2 Reconstruction 18
3.3 Quality evaluation of the acquired data 20
3.4 EIT image parameters 22

3.4.1 Global Inhomogeneity index 23
3.4.2 Local Inhomogeneity index 25
3.4.3 Percentage of pixels inside of $\overline{DI_{lung}} \pm \sigma$ 25
3.5 Data Analysis 26

4 Results and Discussion **27**
4.1 Global Inhomogeneity index 27
4.2 Local Inhomogeneity index 32
4.3 Percentage of pixels inside of $\overline{DI_{lung}} \pm \sigma$ 35
4.4 General Discussion 39

5 Conclusion and Future Work **41**

References **43**

A GREIT figures of merit **49**

B Tidal Images Computed **55**

C Proceeding Paper Published **63**

Chapter 1

Introduction

1.1 Problem Contextualization and Motivation

Chronic obstructive pulmonary disease (COPD) is an umbrella term used to describe chronic lung diseases that cause air flow limitations. The two main types are chronic bronchitis and emphysema. COPD is a major cause of death worldwide, and the burden of this disorder is expected to increase over the next decades (Figure 1.1) [1, 2].

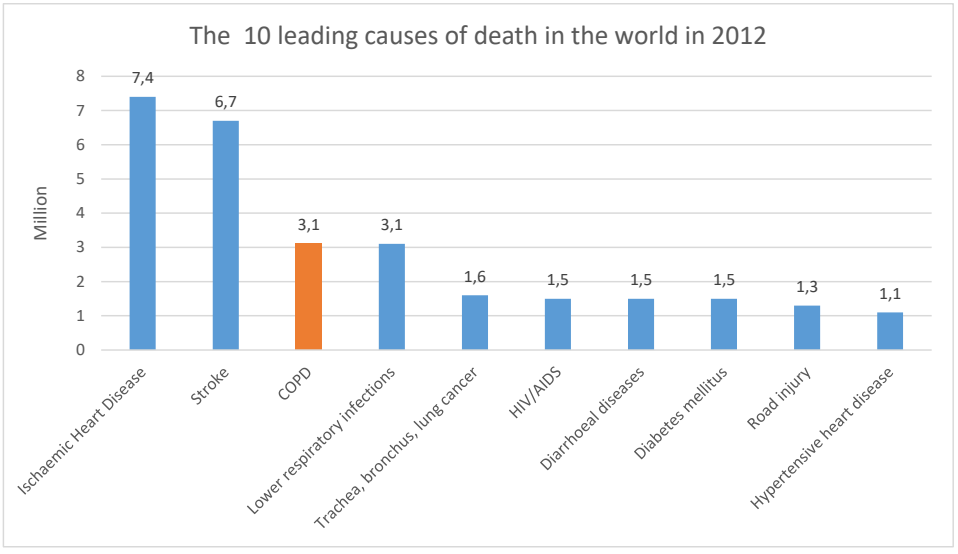

Figure 1.1: COPD was the third leading cause of death in 2012 according to the WHO: 3.1 million died due to this disease [3].

In addition to generating high healthcare costs [4, 5], COPD also causes disability to the patients, having a high impact on their quality of life [6]. The disease is usually progressive [7], meaning the condition of the patient gets gradually worse: its progression rate can be reduced with treatment, but none of the existing medications for COPD has been shown to modify the long-term decline in lung function.

An early diagnosis is therefore essential; tackling the problem early rises life expectancy of the patient and improves his quality of life. However, clinical diagnosis still rely heavily on an appropriate history confirmed by symptomatic spirometry [8]. This has stimulated new research to find novel methods of diagnosis and treatment.

The present study took place within the framework of the WELCOME project (FP7 Grant No. 611223). This project from the European Union aims to develop an integrated care approach for continuous monitoring, early diagnosis and detection of worsening events and treatment of patients suffering from COPD. The intended solution will be based on an adjustable, wearable and washable vest providing continuous monitoring of a large number of sensors, each one measuring various physiological signals allowing a remote, continuous monitoring and analysis of patient multi-parametric data including Electric Impedance Tomography (EIT) [9].

EIT is an imaging technique that seeks to estimate the electrical resistivity distribution inside a body using electrical stimulations and measurements on its surface. Reconstruction algorithms calculate an image from these measurements that reflects the variation in conductivity or impedance within the body. EIT can be applied in several medical areas including pulmonary monitoring [10, 11].

Various developments were accomplished in the last decades in EIT lung monitoring, both in terms of the EIT device design and the image reconstruction algorithm used. There was however, until recently, a lack of research in application specific parameters that extract relevant information to a certain disease or condition from the reconstructed image.

1.2 Objectives

The main focus of this study is the extraction of parameters from the reconstructed EIT images and then the assessment whether these parameters are clinically relevant for COPD diagnosis and monitoring.

1.3 Document Overview

This thesis is structured in five chapters and two appendixes.

Chapter 2 (Background concepts on COPD and EIT lung monitoring): contains information about the impact, risk factors and symptoms of COPD, explains the concept behind EIT and reviews the state of the art around lung EIT monitoring, both in terms of system architecture of the device and image reconstruction algorithms.

Chapter 3 (Materials and Methods): gives a detailed description on how the data was acquired and how images were reconstructed, as well on how the quality of the acquisition of the datasets was evaluated. It also describes the proposed parameters to test and how they were computed.

Chapter 4 (Results and Discussion): presents the statistical analysis of the obtained values for each parameter and presents a discussion of the results obtained.

Chapter 5 (Conclusion and Future Work): evaluates the results of the work, confronts them with the initial objectives and provides suggestions for future work.

Appendix A (GREIT figures of merit): defines the figures of merit used by this reconstruction algorithm, how they are calculated and their desired behaviour.

Appendix B (Tidal Images): contains some of the tidal images computed. One tidal image was computed from each breathing cycle. Each pixel from the tidal image was calculated as the difference between the corresponding pixel in the reconstructed image at end-inspiration and end-expiration.

Appendix C (Proceeding Paper Published): contains the scientific article that resulted from part of the work of this thesis.

1.4 Scientific Contributions

The results obtained during this study resulted in a scientific article presented at the 38th Annual International Conference of the *IEEE Engineering in Medicine and Biology Society*. The article is available in Appendix B.

Chapter 2

Background concepts on COPD and EIT lung monitoring

2.1 COPD: an overview

It is relatively easy to explain what happens physiologically to COPD patients. The air we breath goes down our windpipe into tubes in our lungs called bronchial tubes. Within the lungs, the bronchial tubes divide into many smaller and thinner tubes called bronchioles. These tubes end in groups of minuscule air sacs called alveoli. Due to the elasticity of the air sacs, when you breath in each air sac fills up with air.

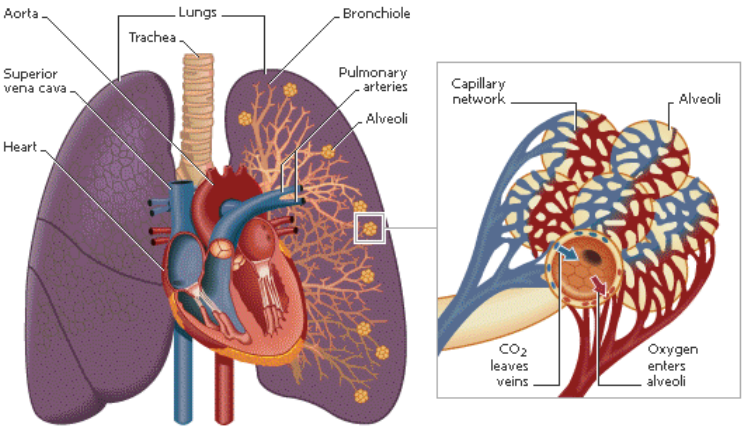

Figure 2.1: Structure of the lung and alveoli. Extracted from [12].

In the lungs of COPD patients there is less air flow in the airways. Depending of the disease this can occur because the walls of the airways become inflamed, the air sacs

lose their elastic quality or there is more production of mucus than usual, which can obstruct these airways [13].

2.1.1 Impact

COPD is a global disease affecting patients worldwide. However, it is especially prevalent in middle-income countries. For each 1000 deaths in the world in 2012, 120 occurred due to COPD: 8 of those in low income countries, 35 in lower-middle, 55 in upper-middle and 22 in high income countries (Figure 2.2).

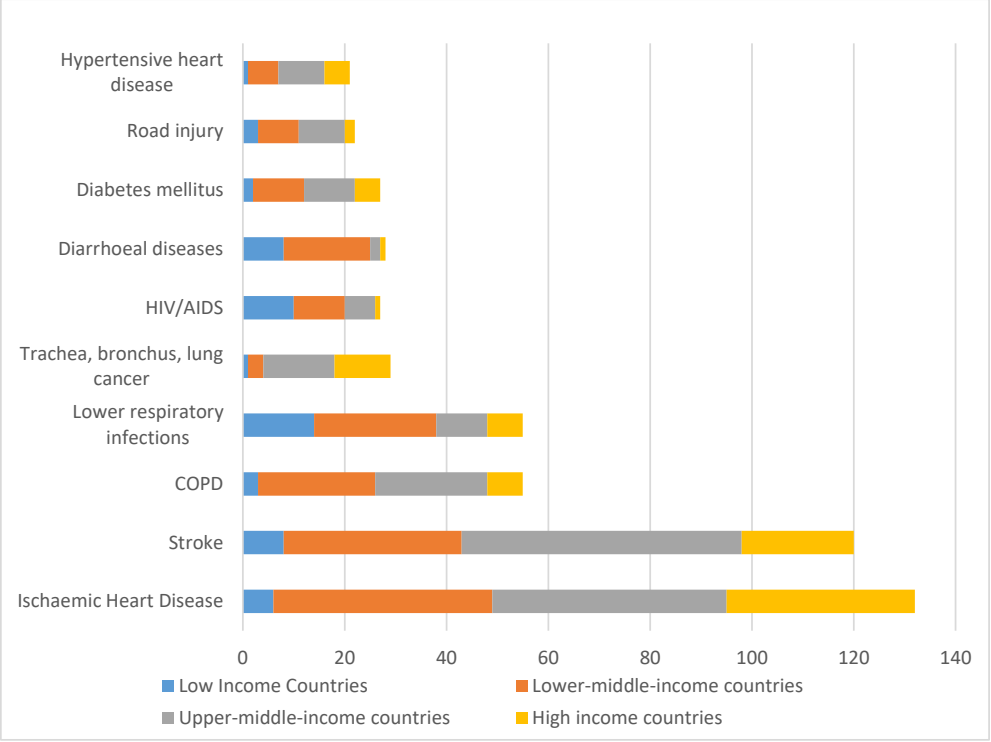

Figure 2.2: Comparison of the top 10 causes of deaths across income groups. COPD is especially prevalent in lower- and upper-middle-income countries [3].

Its impact to the patients' quality of life is made clear by studies like The Global Burden of Disease [14]. This study was an effort to quantify non-fatal health outcomes across an exhaustive set of disorders at the global and regional level, using as a unit years lived with disability (YLDs). According to this report, chronic respiratory diseases accounted for 6.3% of global YLDs, with the largest contributor being COPD, with a total of 29.4 million YLDs [14]. The same report also concludes that the YLDs rates for COPD have risen since 1990.

2.1.2 Risk factors and symptoms

The main risk factor for COPD in high- and middle-income countries is tobacco smoke. In low-income countries exposure to indoor air pollution, such as the use of biomass fuels for cooking and heating, is the main cause [15]. Other risk factors for COPD include the inhalation of occupational dusts and chemicals. Most common COPD symptoms include breathlessness, excessive sputum production and chronic cough [15].

Many patients diagnosed with COPD may also suffer from closely-related chronic diseases including heart failure, diabetes and depression. These co-morbidities add further complexity and cost to public health services, and significantly lower the quality of life for patients suffering from this disease [9]. Thus, COPD patients have complex medical care needs, often involving several treatments as well as self-management responsibilities. This means real-time monitoring of pulmonary ventilation could turn into an important tool for the treatment of patients with COPD.

2.2 EIT and real time monitoring of pulmonary ventilation

Besides having applications in geophysics and industrial process monitoring, over the past decades EIT has been the subject of significant intensive research and has proven to be a reliable tool for monitoring physiological processes in the human body such as cardiac [11] and brain activity [16, 17], gastric emptying [18] or respiration [10, 11].

2.2.1 The general concept behind medical EIT

EIT is an interesting imaging technique for the biomedical field since biological tissues conduct electricity because they contain ions which act as charge carriers [18]. Some tissues conduct electricity better than others because they contain more ions, leading to high resistivity differences between tissue types in the body. The idea behind EIT is to turn the impedance within a body into images, using electrical stimulations and measurements on its surface.

Usually the EIT devices are constituted by a single plane of a number of equidistant electrodes. The measurements are performed by applying an alternating current through

a pair of electrodes while all other remaining electrodes pairs measure potential. The current stimulation is then switched to another pair of electrodes in a sequential process.

A complete set of independent measurements is called a frame, from which an EIT image is calculated via a reconstruction algorithm, and regions of interest (ROIs) identified. From these regions, functional EIT images are generated and application specific EIT parameters calculated (Figure 2.3).

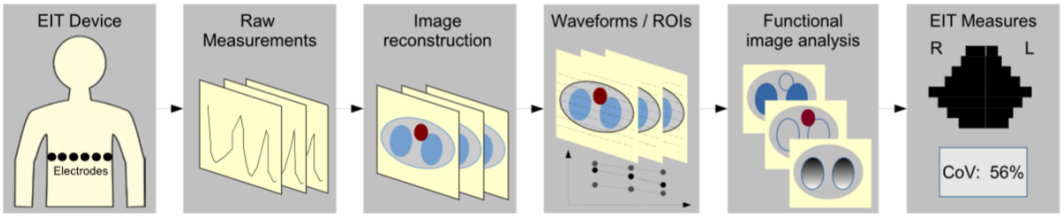

Figure 2.3: Typical steps for EIT data analysis. Extracted from [19].

From the applications in health care one of the first and the current most promising is in real-time monitoring of pulmonary ventilation [10, 11, 20]. This is because lungs are large organs close to the body surface and the lung tissue resistivity is five times higher when compared to most other soft tissues within the thorax (Table 2.1). More importantly, lung resistivity increases and decreases greatly between inspiration and expiration. This results in a high absolute contrast of the lungs in general.

Table 2.1: Typical values of tissue resistivity at a frequency of about 10 kHz [18].

Tissue	**Resistivity** (Ω m)
Muscle	2-4
Fat	20
Lungs	10 (this changes with respiration)
Bone	1.6
Blood	over 40

2.2.2 Applications, opportunities and challenges

There are several reasons that justify the investment in research that has been made around EIT lung monitoring in the last decades. First of all, EIT provides images based on different physical characteristics than other imaging techniques, *i.e.*, it is based on electrical tissue properties. More importantly, EIT, in contrast to all other tomographic imaging techniques, does not apply any kind of ionizing radiation and there are no known

hazards for the patient [21]. Currents typically applied in EIT are relatively small and their frequencies high, not being therefore responsible for any danger to the patient [20]. EIT is also relatively inexpensive compared to other tomographic techniques.

EIT can therefore provide a non-invasive, radiation-free and continuous image of pulmonary impedance which indicates the distribution of ventilation. This makes EIT an ideal candidate for (Figure 2.4):

- bedside monitoring of lung development of pre-term neonates.

  Pre-term neonates often have lung immaturity which can lead to long term health problems. It is therefore important to be able to monitor their lung development in a safe and non-invasive way [22].

- patients in intensive care.

  EIT has been used in critical care medicine as a monitoring tool for a variety of functions such as, but not limited to, monitoring of ventilation distribution [23, 24], detection of pneumothorax [25] and assessment of lung collapse [26, 27] and overdistension [28].

  Mechanical ventilation is often necessary in intensive care medicine. Managing respiration with mechanical ventilation can improve the prognosis of acute phase patients. However, it can produce ventilator induced lung injuries (VILI) or ventilator-associated lung injuries (VALI) [29] and acute respiratory distress syndrome (ARDS) is associated with non-homogeneous lesions in the lungs [30].

  VILI and VALI lead to research into potential solutions, including lung protective ventilation (LPV) strategies. Implementing these strategies requires a tool capable of providing information on the regional behaviour of lungs.

  Generally, chest x-rays and CT have been used for diagnosis of ARDS. However, reaching a diagnosis is hard because the information obtained from a chest x-ray is limited. The patient is therefore often required to undergo a CT examination, which is inconvenient and burdensome for a patient connected to a mechanical ventilator.

- portable continuous monitoring of patients during a long range of time.

  As mentioned before, all of the established medical imaging techniques of lungs apply some kind of ionizing radiation. Long term exposure to radiation would

bring serious hazards to the health of patients, but there are no known hazards for long term lung monitoring using EIT. Furthermore, EIT is cheap and portable [31], making it an attractive option for continuous monitoring of non-clinical patients.

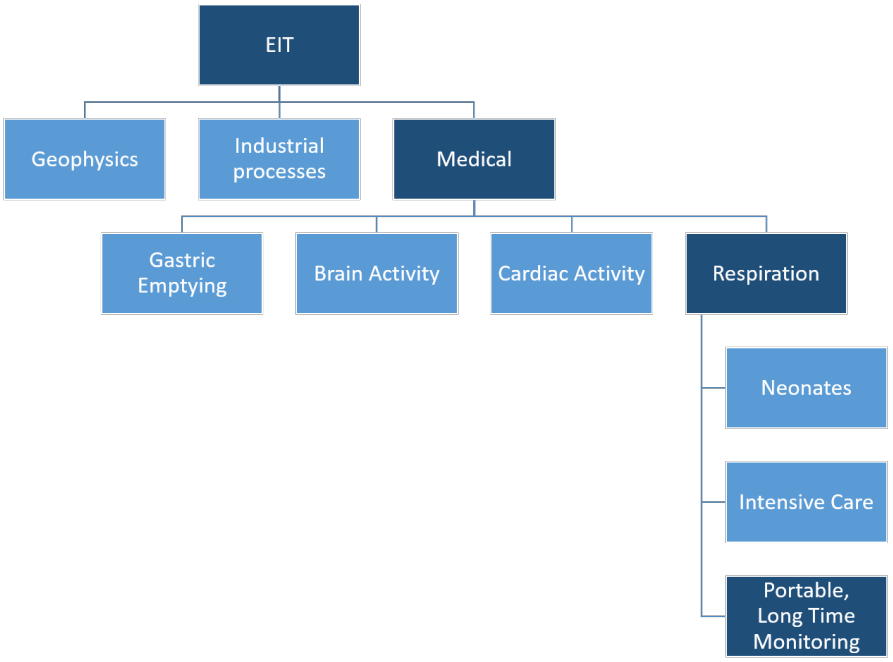

Figure 2.4: Some of the areas of application of EIT.

2.2.2.1 Temporal and spatial resolution

Another factor in favour of EIT is that it is a relatively cheap technique and his temporal resolution (10-50 images per second [10]) can be higher than in other tomographic imaging techniques (around 10 images per second [32]) like x-ray CT or MRI.

Despite all these motivating advantages there are factors that have prevented EIT to become established as a routine tool in healthcare so far. One of the major limitations of EIT is the poor spatial resolution, because of the limited number of independent measurements. Due to the system architecture used in most EIT systems, if N electrodes are used then only $\frac{N(N-3)}{2}$ independent measurements can be made [18].

Most of the architecture systems used in research, including the one used to measure EIT data for this project, have 16 electrodes, limiting the number of independent measurements per frame to 104. This limits greatly the spatial resolution of EIT images. While CT scanners usually provide images consisting of 512×512 pixels, EIT images

from systems using 16 electrodes typically only consist of 32 × 32 pixels [33], thus it is not expected that the spatial resolution of EIT images can be improved in the near future to a point comparable with that of CT.

2.2.2.2 EIT sensitivity and difference imaging

A different limitation of EIT is that it typically shows to be more sensitive to many effects other than the one of interest [19]. The low conductivity lungs act like a shield that prevents current from penetrating to the centre. This effect can be increased by the fat underneath the skin of the patients. On the other hand, EIT is very sensitive to any imperfections in the electronics hardware and the electrode contact.

Another factor to keep in mind is body shape. Image reconstruction from absolute impedance measurements requires knowledge of the exact dimensions and shape of a body as well as the precise electrode location since simplified assumptions would lead to major reconstruction artefacts [34]. The sensitivity of the measurements to body shape is at least as great as the sensitivity to internal resistivity distribution.

EIT researchers avoid this problem by confining their attention only to changes in tissue resistivity and not to absolute values. This was termed difference imaging or functional EIT. A difference image shows the change in tissue resistivity between reference and data points [18]. In this project our reference was the average of the first thirty seconds of the data set.

2.3 EIT System Architecture

EIT systems designed for medical use typically apply high-frequency and low-amplitude current and measure voltage [20]. The single source architecture is the most popular type of EIT devices. These systems normally use only two electrodes at a time for current stimulation, while measurements are made by all electrodes not used for stimulation. But there are also other more complex designs, multifrequency devices, which stimulate current on all electrodes simultaneously and measure voltage at the driven electrodes.

The first EIT system developed for clinical use was the Sheffield Applied Potential Tomograph Mark I, a single source system developed by Barber and Brown in the early

1980s. In this device sixteen electrodes are placed equidistantly around the thorax and one reference electrode is placed on the abdomen. Current is injected at 50 kHz sequentially in adjacent electrode pairs and the potential difference is measured in the remaining electrode pairs [32]. Dynamic images are produced showing the distribution of relative impedance changes. This is done by feeding voltage changes relative to a reference data set into the Sheffield back-projection algorithm [20].

Chest EIT has, due to the high influence of the work by Barber and Brown, most commonly used single source systems. Despite some studies claim that this design has a worse distinguishability performance than other more complex designs, in 2012 around three quarters of the recent EIT designs used the Sheffield protocol [35].

The so called Sheffield protocol follows the design used in the Sheffield Mark I, *i.e.*, the application of a current between two adjacent electrodes and the measurements of the resulting voltage profile between all other adjacent electrodes around the body (Figure 2.5). This process is repeated for current applied between all the adjacent electrode pairs around the body. So, for a system with 16 electrodes, one data frame has current applied from 16 positions, and each position has 13 voltage measurements. The resulting $16 \times 13 = 208$ values, also called a frame, are used to reconstruct one cross-sectional EIT image. There is also one extra electrode, the reference electrode, that is attached to a central point on the chest under investigation. The reference electrode ensures that all measurements at different electrode pair are referenced to the same electric potential.

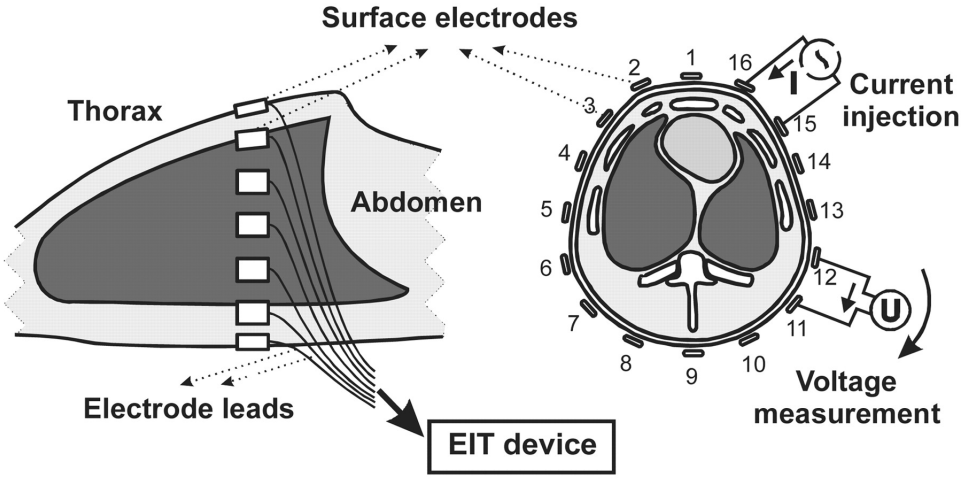

Figure 2.5: Data acquisition of a single source EIT system with 16 electrodes that uses adjacent current stimulation. This system involves application of a current stimulated by the two adjacent electrodes and the measurements of the resulting voltage from all other electrodes around the body. This process is repeated for current applied by each electrode in a clockwise motion. Image extracted from [36].

The EIT system used to acquire data for this project was the Göttingen GOE MF II, developed in the mid-1990s by the EIT Group in Göttingen [37]. This system follows the Sheffield protocol and was a further development step beyond the Sheffield Mark I system. It was the world's first EIT system suited for experimental validation studies in animals and physiological studies in volunteers and clinical research. It is still vastly used in research today.

EIT devices for lung function monitoring designed for everyday clinical use are also already available: Dräger Medical's *Pulmovista 500* [38], since 2010, and Swisstom AG's *Swisstom* BB^2, since 2014 are the most famous examples.

2.4 EIT reconstruction algorithms

The function of a reconstruction algorithm in chest EIT is to transform the voltages measured at the surface of the thorax into a cross-sectional image of impedances.

The problem of recovering conductivity from surface measurements of current and potential is an inverse problem. An inverse problem is the process of calculating from a set of observations the causal factors that produced them. In EIT we want to compute the impedance inside the body that caused the measured potential by the electrodes on the surface. In other words, the objective of an inverse problem is to find the best model y such that:

$$\hat{x} = R(y) \tag{2.1}$$

where R is an operator, often called observation operator, describing the relationship between the observed data, $\hat{x}$, and the model parameters.

For several reasons this is specially challenging in EIT, as described below.

- **Nonlinearity**. In general, the relationship between the distribution of resistivity in the chest and the voltage profile at the boundary is nonlinear. In nonlinear problems, the observation operator cannot be separated to represent a linear mapping of the model parameters that form y into the data, complicating the problem.

Attempts to reconstruct the distribution of resistivity from these profiles without a linearised approximation usually involve a time consuming and iterative solution.

- **Nonlocality**. In conventional medical imaging modalities, such as x-ray CT, a collimated beam of radiation passes through the thorax in a straight line, and the attenuation of this beam is affected only by the matter which lies along its path. In this sense x-ray CT is local, which means that the pixels or voxels of our image affect only a small proportion of the measurements. On the other side, when an electrical current passes through the thorax, the current spreads out in three dimensions, in a direction that is decided by the distribution of impedance inside the thorax. Therefore, any local change in impedance will affect all voltage measurements at the surface of the thorax. This means that, to find the conductivity image, there is the need to solve a system of equations that relates every pixel to every measurement.

- **Ill-posedness**. A mathematical model of a physical problem is well posed if: 1) for all admissible data, a solution exists; 2) for all admissible data, the solution is unique; and 3) the solution depends continuously on the data. The problem in EIT of recovering an unknown conductivity from boundary data is severely ill-posed because of the third criteria: small errors in voltage measurement may lead to drastically different solutions. This is specially significant because of the small number of measurements made due to the limiting number of electrodes from the EIT device.

  This is a serious problem for EIT. An ill-posed problem needs to be re-formulated for numerical treatment. Typically this involves regularization, *i.e.*, including additional assumptions, such as smoothness of the impedance distribution [18]. These assumptions allow decisions between different possible solutions, computing an image that is a reasonably close to the actual impedance distribution within the patients' chest. This reduces however the spatial resolution [39].

2.4.1 Linear reconstruction algorithms

Despite image reconstructions being a nonlinear problem, linearised approximations have been preferred over iterative algorithms in medical EIT.

Some research is currently being conducted in non-linear reconstruction algorithms [40], but these iterative algorithms have not been able to achieve stable results due to the existence of measurement noise and geometric uncertainty [33]. Furthermore, iterative algorithms are too slow for now due to the computational costs. Speed is especially important in EIT because it is one of its main advantages over other available imaging modalities like CT. So, there is still a long road to go until iterative algorithms have a widespread use in EIT.

For these reasons, almost all investigation around EIT lung monitoring, as well as medical EIT in general, is done using linear reconstruction algorithms. Equation 2.1 can, for linear algorithms, be simplified to:

$$\hat{x} = Ry \tag{2.2}$$

2.4.2 Graz consensus Reconstruction algorithm for EIT (GREIT)

During a long time the different versions of the back-projection algorithm implemented in the Sheffield system [41] in the 1980s or the Göttingen system in early 2000s were the most used reconstruction algorithms in medical EIT. These algorithms, despite having been very important for the future of this technique, do not incorporate the advances that have been made over the last years.

For some time a great number of other approaches to linear EIT reconstruction have been proposed [42, 43]. However they have not been widely used because there was a lack of an agreement in the EIT community on which approaches were best, and how they could be combined [33], leading to different algorithms being used by different research groups and different EIT devices.

During the 2007 ICEBI conference in Graz, Austria, initial discussions between the EIT community took place that lead to the development of the GREIT (Graz consensus Reconstruction algorithm for EIT). The objective was to create a reconstruction algorithm that would be accepted by the majority of the experts in EIT algorithm and clinical applications.

GREIT was developed for the following specifications [33, 44]:

- single ring electrode configurations with Sheffield-type EIT systems, using adjacent current injection and measurement (16, 12 or 8 electrodes).
- linear reconstruction of a 2D conductivity change image, based on a 3D forward model.
- reconstruction onto a 32 × 32 pixel array for the following shapes: neonatal chest, male and female adult chest and cylindrical tanks.

The major difference between GREIT and the other reconstruction algorithms is that GREIT is based on a set of performance requirements, in contrast of just being based on a mathematical model which does not factor in those performance requirements [33]. GREIT has therefore performance requirements encoded into the algorithm, established after discussion with different experts in the medical EIT area. These figures of merit are described in Appendix A.

To reconstruct the images from EIT data correctly, GREIT needs a forward model, a noise model and the desired performance metrics. What information each model provides to the reconstruction model is explained below. An extensive and detailed mathematical description on how the algorithm implements these informations and the performance metrics can be read in Adler *et al* 2009 [33].

The body under investigation is modelled using a forward model. The models represent the details of the body geometry, the electrode size, placement and contact impedance. A forward model allows calculation of EIT measurement data from a conductivity change distribution. With a correct forward model, and knowing X, one can calculate Y in Equation 2.2.

The noise model allows an estimation of representative noise samples from EIT measurements. It considers two sources of noise. Electronic measurement noise is considered and modelled to be uniform and Gaussian in EIT. Electrode movement artefacts occur with movement of the electrodes, that can occur with chest movements of the patients due to breathing or a posture change.

Chapter 3

Materials and Methods

3.1 Data Acquisition

Datasets from adult subjects were acquired on three different occasions by a team composed of researchers, nurses and medical doctors. Two of those occasions were at the General Hospital of Thessaloniki, Greece, and one at University Medical Centre Schleswig-Holstein, Campus Kiel, Kiel, Germany. A total of 26 subjects were examined: 12 healthy subjects (38.3 ± 7.3 years old, mean age ± SD; female/male: 7/5) and 14 patients with diagnosis of COPD (72.8 ± 8.3 years old; female/male: 2/12). All data relevant for this study was acquired during tidal breathing.

During these acquisitions sixteen self-adhesive electrodes (Blue Sensor L-00-S, Ambu, Ballerup, Denmark) were attached on the chest circumference in the 5-6th intercostal space and one reference electrode on the abdomen in each studied subject.

Measurements involved application of a current (50 kHz, 5 mA$_{rms}$) between two adjacent electrodes, while the voltage is measured by the rest of the electrodes. This process is repeated for current applied between all the adjacent electrode pairs around the body in a sequential process. The EIT data were acquired using the Goe-MF II EIT device (CareFusion, Höchberg, Germany) at around 33 images/s.

This study was approved by the institutional ethics committee and informed written consent was obtained from each study participant.

3.2 Reconstruction

Images were reconstructed from the obtained data using the GREIT algorithm [33]. Reconstruction was done with the help of EIDORS [45]. EIDORS is an open-source software tool box written mainly in MATLAB designed for image reconstruction from EIT data. It has been used both in lung imaging as well as other medical imaging applications like measuring cardiac activity and imaging electrical activity in the brain. The software also has a list of forward models, needed for the reconstruction, created using the finite element method. An adult thorax shaped model with a single plane of 16 electrodes and adjacent stimulation pattern was selected from the model library.

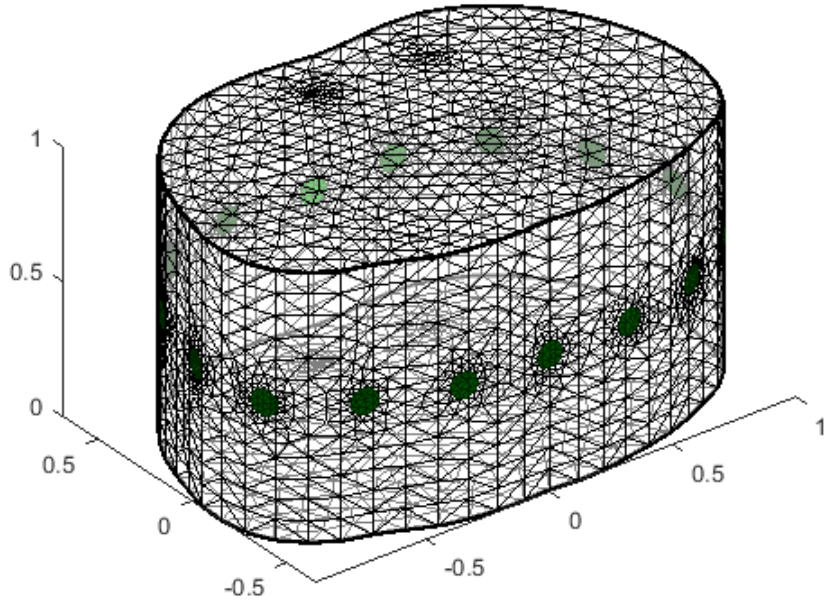

Figure 3.1: Adult thorax shaped model selected from the model library [45].

The obtained EIT images consist of 32 × 32 pixels, but only 912 of those are pixels of interest, representing the inside of the thorax. The value on each pixel represent the normalised difference between the instantaneous and the reference impedance for that location. Our reference value was calculated as the average of the first thirty seconds of that data set.

For each data set the GIC (global impedance curve) over time was obtained, by calculating for each frame or image the sum of all of his pixels (Figure 3.2).

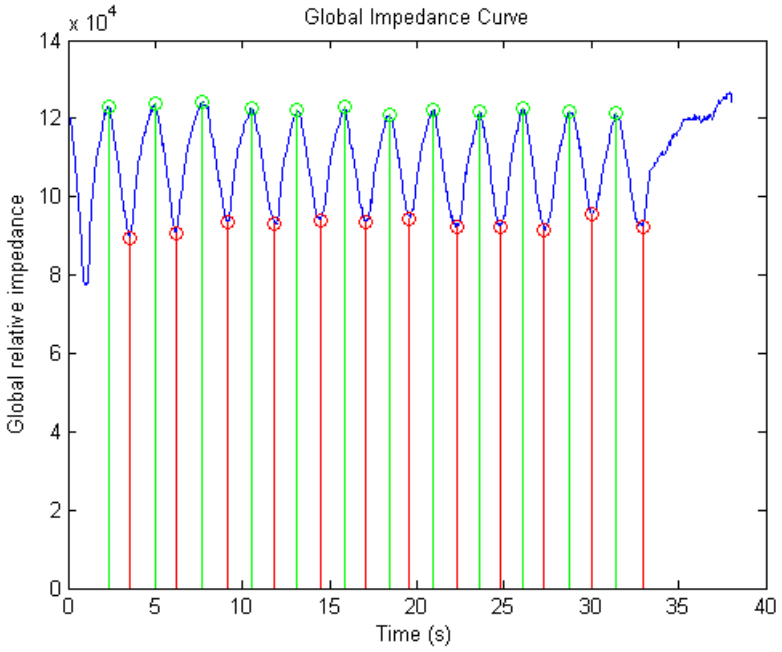

Figure 3.2: GIC obtained of one dataset. The end-inspiration (green dots) and end-expiration (red dots) moments are found from this curve.

From this information, end-inspiration and end-expiration moments were identified. At end-inspiration the lungs are filled with air and the total impedance value reaches a maximum. At end-expiration the opposite occurs.

From this, a tidal EIT image was computed for each breathing cycle. Each pixel from the tidal EIT image was calculated as the difference between the corresponding pixel in end-inspiration and in end-expiration.

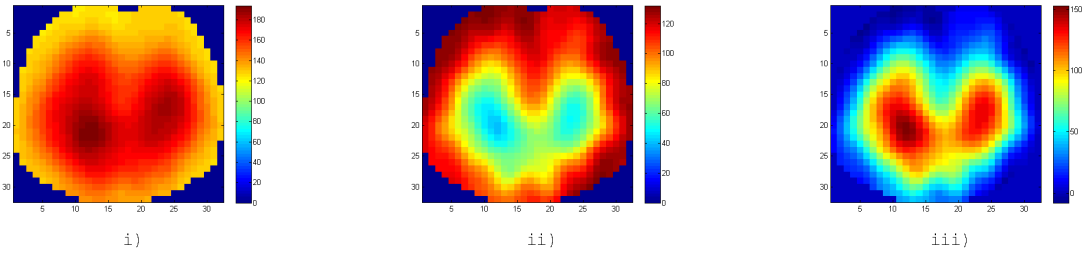

Figure 3.3: Obtained image at: i) end-inspiration; ii) the following end-expiration and iii) the resulting tidal image.

Each pixel in the tidal EIT image represents the value of impedance difference between the two moments. In the lung area this approximately represents the difference in volume of air between inspiration and expiration.

3.3 Quality evaluation of the acquired data

Not all acquired data is suitable for analysis. For various reasons, as for example bad electrode placing and coughing, speaking or movement during acquisition, between others, some datasets may have more noise or measure smaller impedance differences between end inspiration and end expiration than expected. This will affect the result of the evaluation of the studied parameter and these datasets should therefore not be used.

It is therefore important to find means to evaluate the quality of the acquisition before using the dataset to test parameters and make conclusions about their usefulness for COPD testing and monitoring.

A first idea on the quality of the acquisition can be obtained by looking at the GIC of the data set. Figure 3.2 shows what the GIC of a near ideal acquisition looks like, while Figure 3.4 shows the GIC of an acquisition with an unacceptable amount of noise and Figure 3.5 shows the GIC of an acquisition which measured smaller impedance differences than normal.

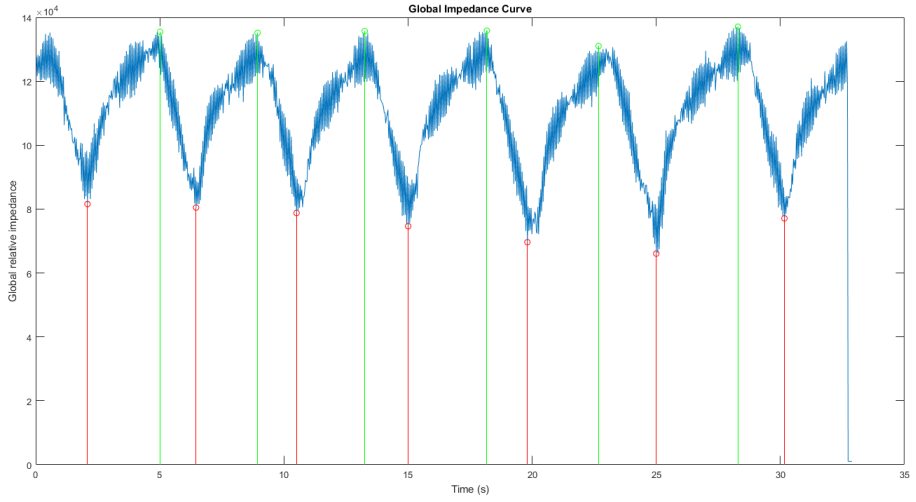

Figure 3.4: Global impedance curve obtained for one dataset with an unacceptable amount of noise.

To evaluate the datasets two parameters were computed: the average pixel difference (APD) from all tidal images of each dataset and the noise.

To obtain the APD of each dataset we first computed the average pixel value of each tidal image. Then we calculated the average of these values:

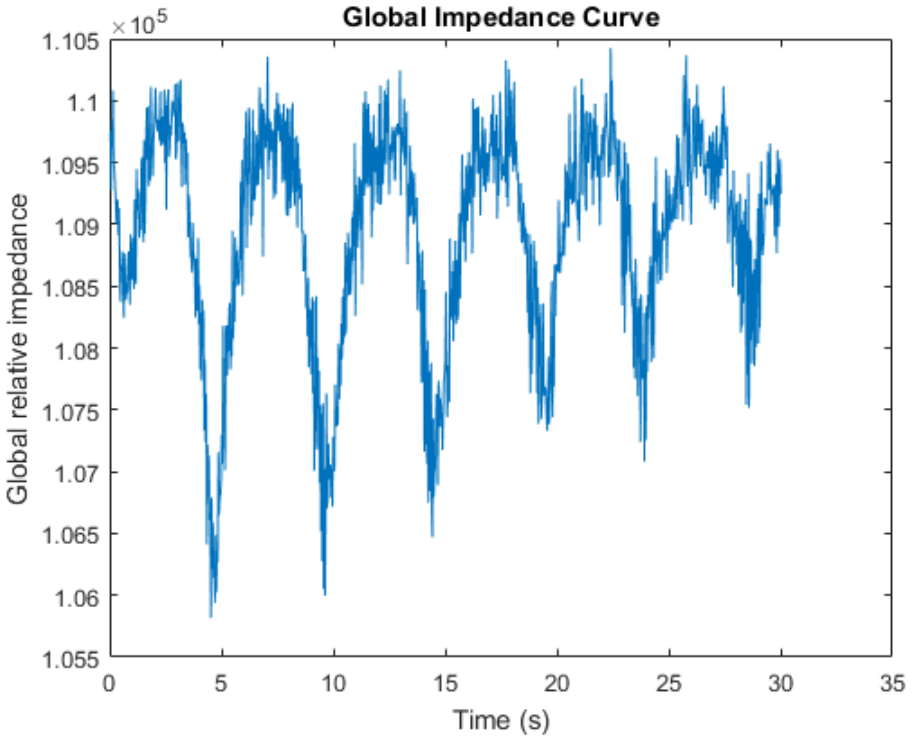

Figure 3.5: Global impedance curve obtained for one dataset with small impedance differences during acquisitions. Differences between end inspiration and end expiration are only around $3 - 5 \times 10^3$ for this data set, much lower than for other acquisitions (around 3×10^4, as can be seen in Figure 3.2 and Figure 3.4).

$$APD = \frac{\sum_{breathingcycle} \frac{\sum DI_{x,y}}{\#pixels}}{N_{bc}} \tag{3.1}$$

where $DI_{x,y}$ is the value of the pixel x, y from the tidal image, $\#pixels$ is the number of pixels that every tidal image has ($32 \times 32 = 1024$) and N_{bc} is the number of breathing cycles (or tidal images) available from that dataset.

For the noise calculation, first a Fast Fourier Transform (FFT) was computed for the global impedance curve. Then the values between 3 Hz (value chosen after careful observation of the amplitude spectrum of the FFT, Figure 3.6) and half of the frame rate of the acquisition were added.

The obtained results are shown in Tables 3.1 and 3.2. Datasets with an APD under 10 or Noise over 10^5 (bold values on the table) were considered not suitable. This threshold excluded healthy subjects #1 to #4, #11 and #12, one dataset from healthy subject #6 and patient #14 and two datasets from patient #3.

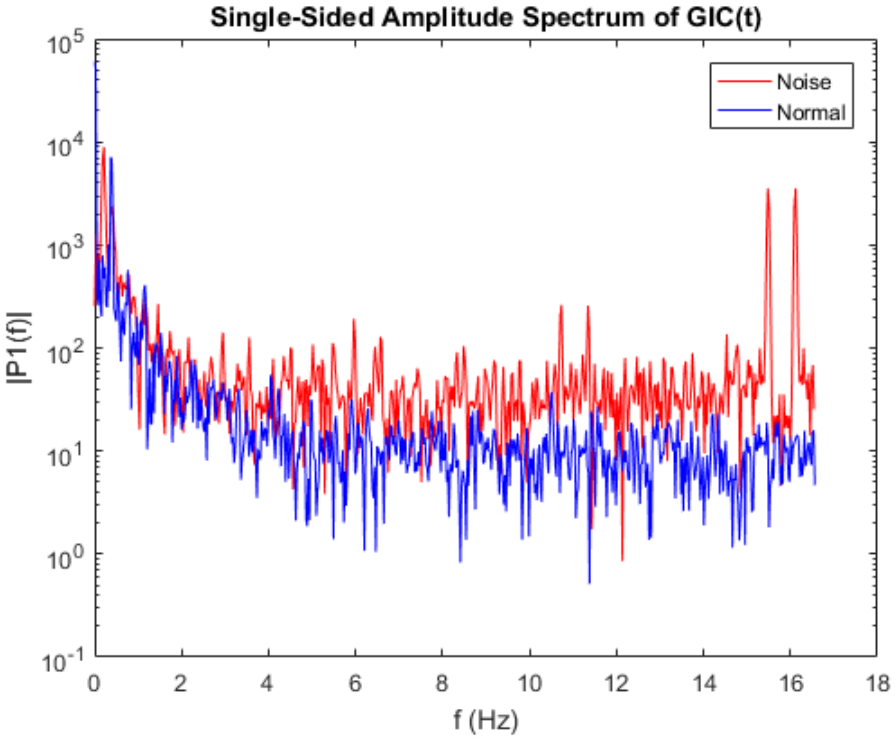

Figure 3.6: FFT spectrum for the global impedance curve of a dataset with normal noise (in blue) and excessive noise (in red).

3.4 EIT image parameters

While the generation of EIT images can in itself give important medical information, application possibilities are not limited to it. Quantitative parameters that characterizes the state of the lungs can also be computed from EIT data. The aim of this study was to implement three EIT parameters and test their usefulness in COPD diagnosis and monitoring.

To calculate these parameters the lung area was first of all identified for each tidal image. The lung areas were estimated using functional EIT with a predefined threshold of 35%, i.e., pixels with values larger than 35% of the maximum value in that image were identified as lung area. Since the lungs are expected to be relatively symmetric, the lung area identified was mirrored from left to right and from right to left and combined by a logical OR operation. The final resulting area was considered to represent the lung area for each parameter.

Table 3.1: Evaluation of the data acquisition quality of healthy subjects.

Subject	Dataset	Noise ($\times 10^4$)	Average Pixel Difference
1	1	**15.1**	**10**
2	1	**18.4**	**5**
3	1	3.6	**10**
4	1	**15.1**	18
5	1	2.9	15
6	1	1.9	45
	2	1.0	41
	3	**10.0**	45
7	1	0.9	36
	2	2.7	68
	3	9.6	79
8	1	1.7	46
	2	1.2	36
	3	1.4	38
9	1	8.7	42
	2	8.2	35
	3	3.0	63
10	1	1.0	12
	2	1.2	20
11	1	**12.9**	19
	2	**11.7**	17
12	1	**11.4**	**4**
	2	**12.2**	**4**

3.4.1 Global Inhomogeneity index

The global inhomogeneity (GI) index is an EIT parameter that quantifies the tidal volume distribution within the lung [46].

The GI index has been used mainly with patients under mechanical ventilation in mind, in particular ARDS patients [47–49], and has shown to be reliable and interpatient comparable [47]. This parameter is calculated from tidal EIT images. To the best of our knowledge this is the first time someone evaluates the viability of this parameter for COPD patients during tidal breathing.

The median value of the pixels in the identified lung area is computed. The sum of the absolute difference between the median value and every pixel value is considered to represent the variation in tidal volume distribution in the whole lung region [46]. To make the GI index universal and interpatient comparable, it is normalized to the sum of the impedance values within the lung area:

Table 3.2: Evaluation of the data acquisition quality of the COPD patients.

Patient	Dataset	Noise ($\times 10^4$)	Average Pixel Difference
1	1	7.1	25
	2	2.8	35
	3	7.8	39
2	1	3.1	46
	2	8.6	40
	3	1.8	28
3	1	**11.1**	74
	2	**11.1**	77
	3	4.5	50
4	1	6.7	33
	2	1.6	35
5	1	1.7	34
	2	8.5	24
6	1	1.6	17
	2	2.4	39
	3	9.5	37
7	1	7.9	25
	2	1.1	39
8	1	8.9	34
	2	2.5	37
	3	8.5	35
9	1	7.7	34
	2	3.5	68
10	1	9.0	24
	2	8.0	25
	3	8.6	34
11	1	8.2	31
	2	2.4	28
	3	9.6	32
12	1	2.8	30
	2	2.1	25
	3	2.8	56
13	1	3.7	20
	2	9.6	28
	3	6.5	31
14	1	**10.6**	36
	2	7.7	41
	3	9.2	43

$$GI = \frac{\sum_{x,y \in lung} |DI_{x,y} - Median(DI_{lung})|}{\sum_{x,y \in lung} DI_{xy}} \tag{3.2}$$

where $\mathrm{DI}_{x,y}$ is the value of the differential impedance for the pixel at x, y in the tidal image and DI_{lung} represents all the pixels considered to be part of the lung area.

3.4.2 Local Inhomogeneity index

The LI index was proposed by the same group that first implemented the GI index [46]. Both intend to quantify lung inhomogeneity by evaluating the lung area of tidal images and were created with patients under mechanical ventilation in mind. The main difference between the two indices is that, while the GI index aims to characterize lung ventilation homogeneity in a global level, the LI index focuses on local inhomogeneity, calculating differences between neighbouring pixels. This index is normalized using the same approach as for GI, by dividing by the sum of the impedance values within the lung area.

The LI index is described by the following equation:

$$LI = \sum_{x,y \in lung} \left(\frac{1}{m-1} \times \sum_{i,j \in [-1,1] \bigcap x+i, y+j \in lung} |DI_{xy} - DI_{x+i,y+j}| \right) \div \sum_{x,y \in lung} DI_{xy} \tag{3.3}$$

where DI_{xy} is the value of the pixel x, y in the identified lung area; $DI_{x+i,y+j}$ are the neighbour pixels of $DI_{x,y}$ and finally m is the length of $i, j \in [-1, 1] \bigcap x + i, y + j \in lung$ or simply the amount of neighbour pixels that are part of the lung area.

3.4.3 Percentage of pixels inside of $\overline{DI_{lung}} \pm \sigma$

We consider that testing the viability of the GI and LI indexes in COPD testing and monitoring makes sense because they measure lung ventilation inhomogeneity, which is a direct consequence of the air flow limitations caused by this disease.

Following this logic, we intended to implement and test another parameter that also presents information about the patients' breathing but in a different way.

This parameter can be described as the percentage of pixels inside $\overline{DI_{lung}} \pm \sigma$, where $\overline{DI_{lung}}$ is the average of all pixels that are part of the lung area of the tidal image and σ is the standard deviation of those values (Equations 3.4 and 3.5). This parameter will be referred by the acronym PoP from now on.

$$PoP = \frac{\sum_i^N DI_i}{N} \tag{3.4}$$

where DI_i is equal to:

$$DI_i \begin{cases} 1 & \text{if } DI_i \in \left[\overline{DI_{lung}} - \sigma, \overline{DI_{lung}} + \sigma\right] \\ 0 & \text{else} \end{cases} \tag{3.5}$$

where DI_i is the value of the ith pixel part of the lung area, $\overline{DI_{lung}}$ is the average value of all pixels inside the lung area, σ is the standard deviation of those values and N is the number of pixels considered to be part of the lung area.

3.5 Data Analysis

For each breathing cycle acquired a tidal image was computed and the three different parameters described in the previous chapter were calculated for both patients and healthy subjects. Because there is one measurement variable (value obtained for the parameter) and one nominal variable (control or COPD), no certainty that the data follows a normal distribution and a small sample size in terms of data, the obtained results were compared using the Kruskal-Wallis test. A p value <0.05 was considered to reject the null hypothesis: "values from the control and from the COPD group are drawn from the same distribution".

The receiver operating characteristic (ROC) curve was computed for each parameters to evaluate their classification performance. The curve is created by plotting the true positive rate against the false positive rate at different thresholds. The area under curve (AUC) is equal to the probability that a random value of the COPD group is higher than a random value of the control group, so a parameter with an AUC of 0.5 would classify a value correctly as control or COPD only 50% if the time. In other words, the higher the AUC is, the better is the classification performance of the parameter.

Data analysis was performed using MATLAB 8.3 (The Mathworks, Natick, MA, USA).

Chapter 4

Results and Discussion

The content in this chapter presents the data analysis described in section 3.5, as well as a discussion of the obtained results.

4.1 Global Inhomogeneity index

Table 4.1 presents the average GI, as well as the number of breathing cycles analysed for each dataset of the control group. Table 4.2 displays the same information, but for the COPD group. Data are presented as mean and standard deviation (SD). The overall average GI obtained was 0.78 ± 0.15 for the control group and 0.85 ± 0.20 for the COPD group.

The GI values obtained for the COPD patients were compared to the control group using the Kruskal-Wallis test (Figure 4.1). The p value returned from the test ($p = 7.98 \times 10^{-7}$) is lower than the significance level, thus rejecting the null hypothesis described in section 3.5.

There are, however, significantly more subjects for our COPD group than for the control group. The control group has 6 subjects with a total of 99 breathing cycles, while the COPD group has 14 subjects with a total of 318 breathing cycles. Due to the existence of unbalanced groups, a Monte Carlo cross validation was done. This was achieved by selecting 100 times 99 random GI values from the COPD group and comparing them with the 99 GI values from the control group using the Kruskal-Wallis test. The 100 p values

Table 4.1: Average GI obtained for each dataset of the control group.

Subject	Dataset	$\overline{GI}$	SD	# Breathing Cycles
5	1	0.98	0.05	6
6	1	1.03	0.03	12
	2	0.97	0.03	12
7	1	0.70	0.05	12
	2	0.65	0.01	7
	3	0.67	0.01	7
8	1	0.65	0.01	5
	2	0.73	0.03	6
	3	0.67	0.02	6
9	1	0.65	0.03	5
	2	0.66	0.03	6
	3	0.66	0.04	8
10	1	0.75	0.00	3
	2	0.70	0.05	4

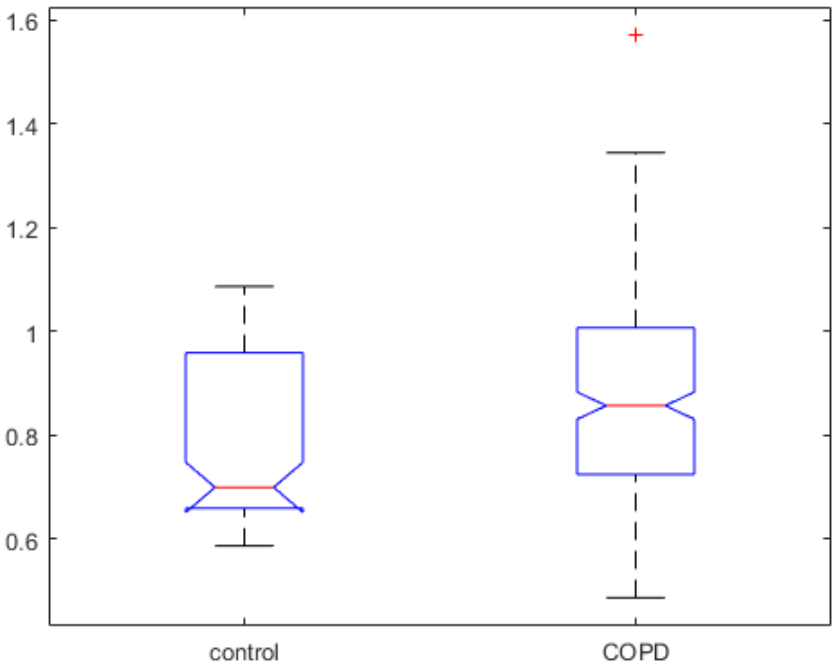

Figure 4.1: Comparison of the obtained GI values for the COPD patients and the control group. The boxes mark the quartiles while the whiskers extend from the box out to the most extreme data value within 1.5x the interquartile range of the sample. The red crosses represent outliers.

Table 4.2: Average GI obtained for each dataset of the COPD group.

Patient #	Dataset	$\overline{GI}$	SD	# Breathing Cycles
1	1	0.96	0.07	11
	2	0.95	0.06	10
	3	1.01	0.05	9
2	1	0.89	0.05	6
	2	0.80	0.05	8
	3	0.82	0.10	6
3	3	0.77	0.14	9
4	1	0.93	0.06	7
	2	0.93	0.05	7
5	1	0.72	0.03	8
	2	0.88	0.09	8
6	1	0.81	0.08	6
	2	0.71	0.03	6
	3	0.75	0.03	9
7	1	0.75	0.05	9
	2	0.73	0.03	10
8	1	0.64	0.07	6
	2	0.56	0.03	7
	3	0.57	0.04	8
9	1	0.94	0.08	9
	2	0.80	0.05	9
10	1	1.21	0.15	10
	2	1.19	0.07	10
	3	1.15	0.09	10
11	1	0.82	0.08	9
	2	0.92	0.08	12
	3	0.78	0.07	15
12	1	0.54	0.06	10
	2	0.64	0.04	12
	3	0.55	0.04	8
13	1	1.14	0.07	12
	2	1.06	0.12	10
	3	1.01	0.07	12
14	2	0.66	0.03	8
	3	0.69	0.03	12

obtained are represented in Figure 4.2, with all of them being lower than the significance level. These results support the conclusion that there is a consistent difference between the GI values obtained from the COPD group and the control group.

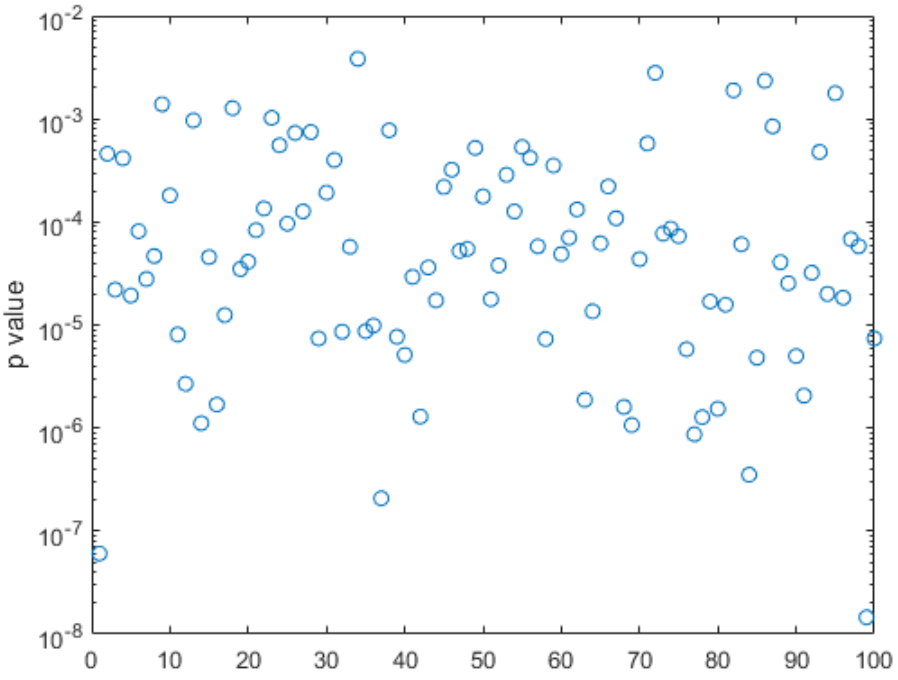

Figure 4.2: Representation of the obtained p values during cross validation. Highest p value obtained: $p_{max} = 3.8 \times 10^{-3}$.

An analysis between the groups for each gender was done as well. The result of the cross validation between the control group and the COPD group for the female population and male population are presented in Figure 4.3 and Figure 4.4, respectively.

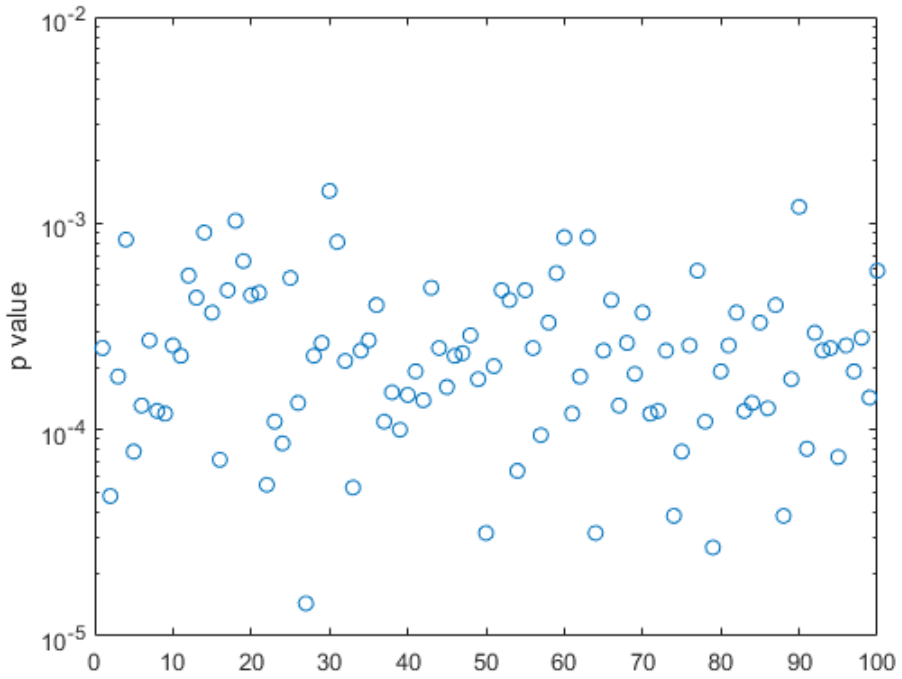

Figure 4.3: Representation of the obtained p values during cross validation between the GI values of the female control group and the female COPD group. Highest p value obtained: $p_{max} = 1.4 \times 10^{-3}$.

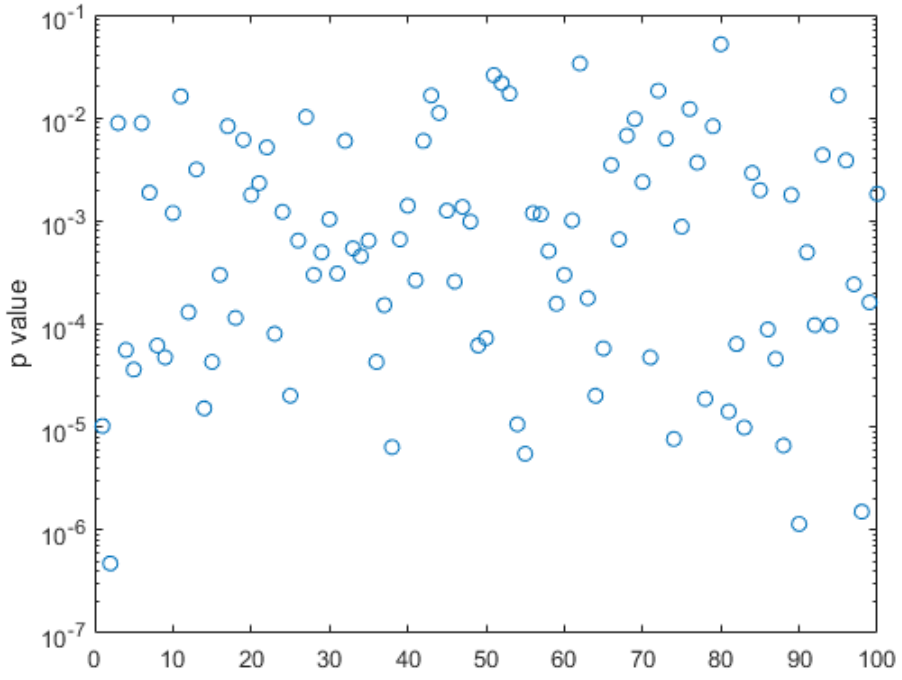

Figure 4.4: Representation of the obtained p values during cross validation between GI values of the male control group and the male COPD group. Highest p value obtained: $p_{max} = 5.2 \times 10^{-2}$.

4.2 Local Inhomogeneity index

The average LI for each dataset of the control group and the COPD group are presented in Table 4.3 and Table 4.4, respectively. The overall average LI obtained was 0.20 ± 0.04 for the control group and 0.21 ± 0.05 for the COPD group.

Table 4.3: Average LI obtained for each dataset of the control group.

Subject	Dataset	$\overline{LI}$	SD	# Breathing Cycles
5	1	0.22	0.01	6
6	1	0.27	0.01	12
	2	0.24	0.01	12
7	1	0.19	0.01	12
	2	0.16	0.00	7
	3	0.16	0.01	7
8	1	0.17	0.00	5
	2	0.19	0.01	6
	3	0.18	0.01	6
9	1	0.18	0.01	5
	2	0.17	0.02	6
	3	0.18	0.01	8
10	1	0.17	0.00	3
	2	0.16	0.01	4

The result of the Kruskal-Wallis test can be seen in Figure 4.5. The returned p value (1.16×10^{-2}) is lower than the significance level.

A Monte Carlo cross validation was performed for this parameter, for the same reason and following the same method that was described in the GI section (Figure 4.6). From the 100 simulations, a total of 43 p values were obtained over the threshold value, with the highest being $p_{max} = 4.98 \times 10^{-1}$. We therefore can not claim with a high confidence that the values from the two groups come from different distributions.

These results leave little hope for the use of the LI index as a viable parameter for identification and monitoring of COPD condition.

Table 4.4: Average LI obtained for each dataset of the COPD group.

Patient	Dataset	$\overline{LI}$	SD	# Breathing Cycles
1	1	0.22	0.01	11
	2	0.21	0.01	10
	3	0.23	0.01	9
2	1	0.21	0.01	6
	2	0.19	0.02	8
	3	0.18	0.02	6
3	3	0.16	0.03	9
4	1	0.21	0.01	7
	2	0.19	0.01	7
5	1	0.20	0.01	8
	2	0.22	0.02	8
6	1	0.22	0.05	6
	2	0.19	0.01	6
	3	0.19	0.01	9
7	1	0.22	0.02	9
	2	0.19	0.01	10
8	1	0.19	0.02	6
	2	0.18	0.02	7
	3	0.16	0.02	8
9	1	0.23	0.01	9
	2	0.19	0.01	9
10	1	0.29	0.04	10
	2	0.28	0.02	10
	3	0.27	0.03	10
11	1	0.19	0.01	9
	2	0.21	0.02	12
	3	0.18	0.02	15
12	1	0.14	0.01	10
	2	0.15	0.01	12
	3	0.15	0.01	8
13	1	0.34	0.03	12
	2	0.30	0.04	10
	3	0.26	0.03	12
14	2	0.16	0.01	8
	3	0.17	0.01	12

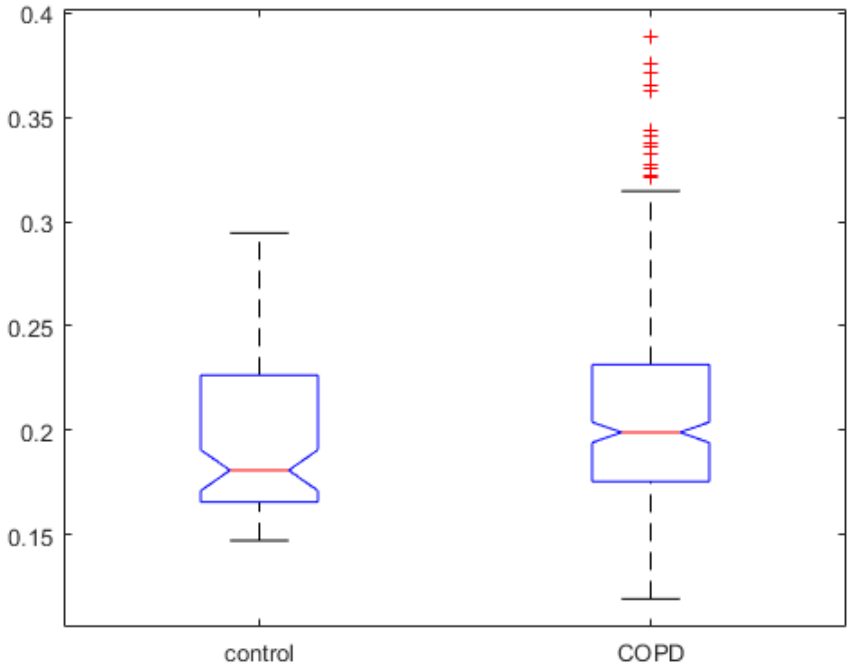

Figure 4.5: Comparison of the LI values for the COPD patients and the control group.

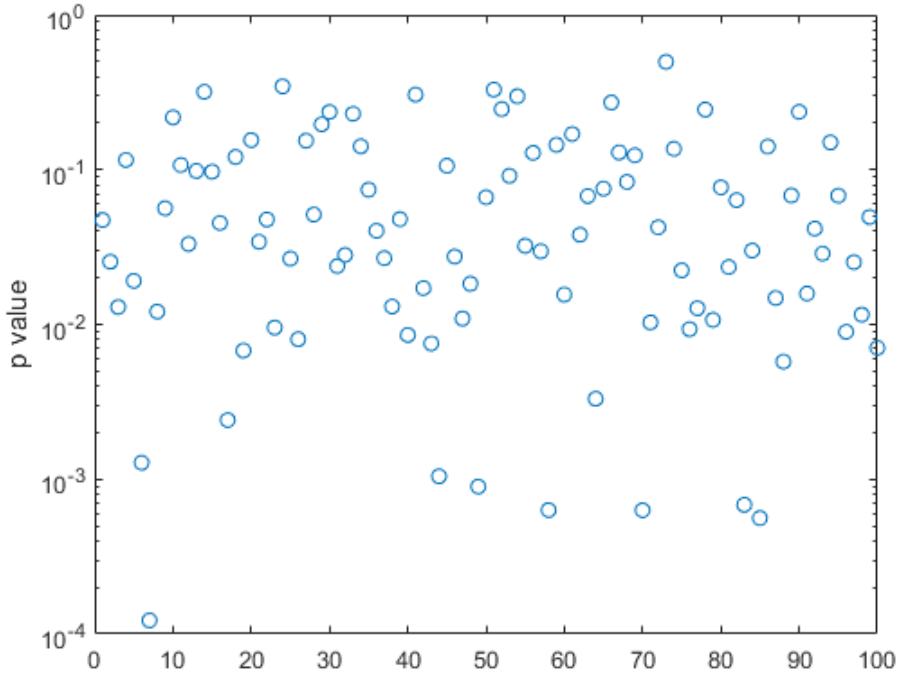

Figure 4.6: Representation of the obtained p values during cross validation. Highest p value obtained: $p_{max} = 4.98 \times 10^{-1}$.

Table 4.5: Average PoP obtained for each dataset of the control group.

Subject	Dataset	$\overline{PoP}$	SD	# Breathing Cycles
5	1	0.61	0.01	6
6	1	0.65	0.03	12
	2	0.62	0.01	12
7	1	0.71	0.05	12
	2	0.62	0.02	7
	3	0.61	0.03	7
8	1	0.66	0.02	5
	2	0.66	0.02	6
	3	0.68	0.01	6
9	1	0.61	0.02	5
	2	0.63	0.04	6
	3	0.63	0.02	8
10	1	0.64	0.01	3
	2	0.59	0.02	4

4.3 Percentage of pixels inside of $\overline{DI_{lung}} \pm \sigma$

The average PoP for each dataset of the control group and the COPD group are presented in Table 4.5 and Table 4.6, respectively. The overall average PoP obtained was 0.64±0.04 for the control group and 0.69 ± 0.06 for the COPD group.

The Kruskal-Wallis test returned a p value far below the considered threshold (Figure 4.7, $p = 2.78 \times 10^{-15}$).

A Monte Carlo cross validation was performed for this parameter, for the same reason and following the same method that was described in the GI section. All the p values returned from the cross validation are lower than the significance level (Figure 4.8).

An analysis between the groups for each gender was done as well. The result of the cross validation between the control group and the COPD group for the female population and male population are presented in Figure 4.9 and Figure 4.10, respectively. For both gender the returned p values are lower than the significance level.

Table 4.6: Average PoP obtained for each dataset of the COPD group.

Patient	Dataset	$\overline{PoP}$	SD	# Breathing Cycles
1	1	0.68	0.08	11
	2	0.64	0.03	10
	3	0.67	0.03	9
2	1	0.66	0.03	6
	2	0.64	0.04	8
	3	0.58	0.03	6
3	3	0.61	0.02	9
4	1	0.70	0.03	7
	2	0.70	0.05	7
5	1	0.68	0.03	8
	2	0.76	0.02	8
6	1	0.68	0.02	6
	2	0.75	0.02	6
	3	0.75	0.03	9
7	1	0.68	0.03	9
	2	0.66	0.02	10
8	1	0.72	0.04	6
	2	0.73	0.06	7
	3	0.66	0.02	8
9	1	0.71	0.02	9
	2	0.66	0.02	9
10	1	0.75	0.02	10
	2	0.73	0.03	10
	3	0.73	0.02	10
11	1	0.72	0.04	9
	2	0.70	0.05	12
	3	0.67	0.02	15
12	1	0.64	0.04	10
	2	0.61	0.03	12
	3	0.65	0.03	8
13	1	0.70	0.04	12
	2	0.72	0.04	10
	3	0.70	0.02	12
14	2	0.71	0.04	8
	3	0.76	0.04	12

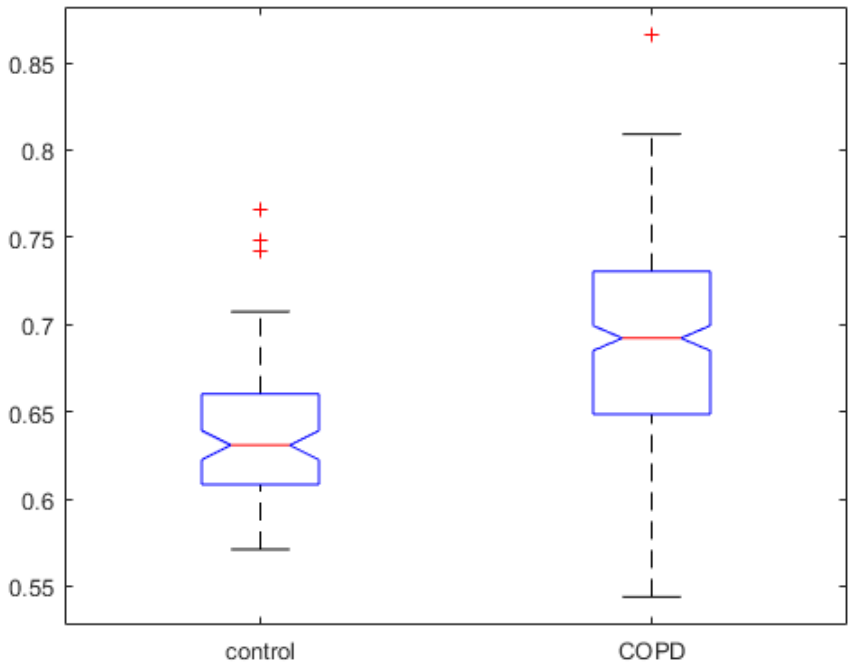

Figure 4.7: Comparison of the obtained PoP values for the COPD patients and the control group.

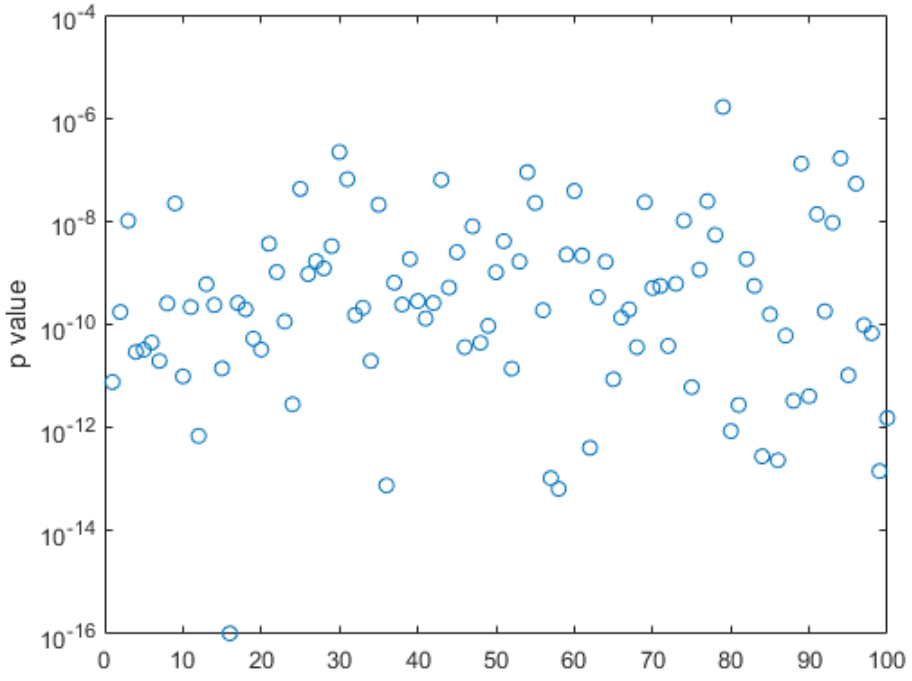

Figure 4.8: Representation of the obtained p values during cross validation. Highest p value obtained: $p_{max} = 1.6 \times 10^{-6}$.

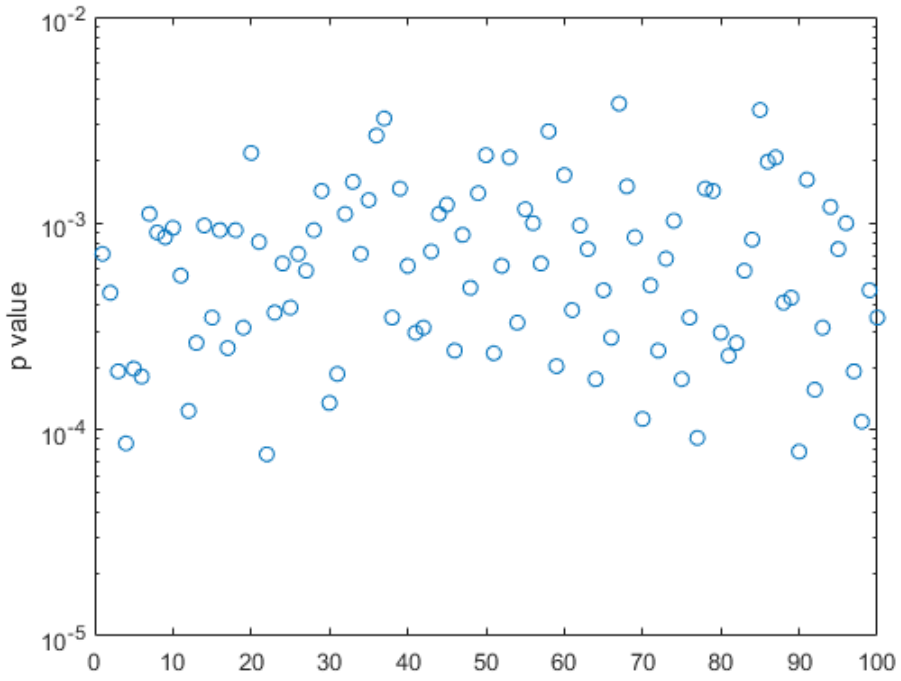

Figure 4.9: Representation of the obtained p values during cross validation between the PoP results obtained for the female control group and the female COPD group. Highest p value obtained: $p_{max} = 3,8 \times 10^{-3}$.

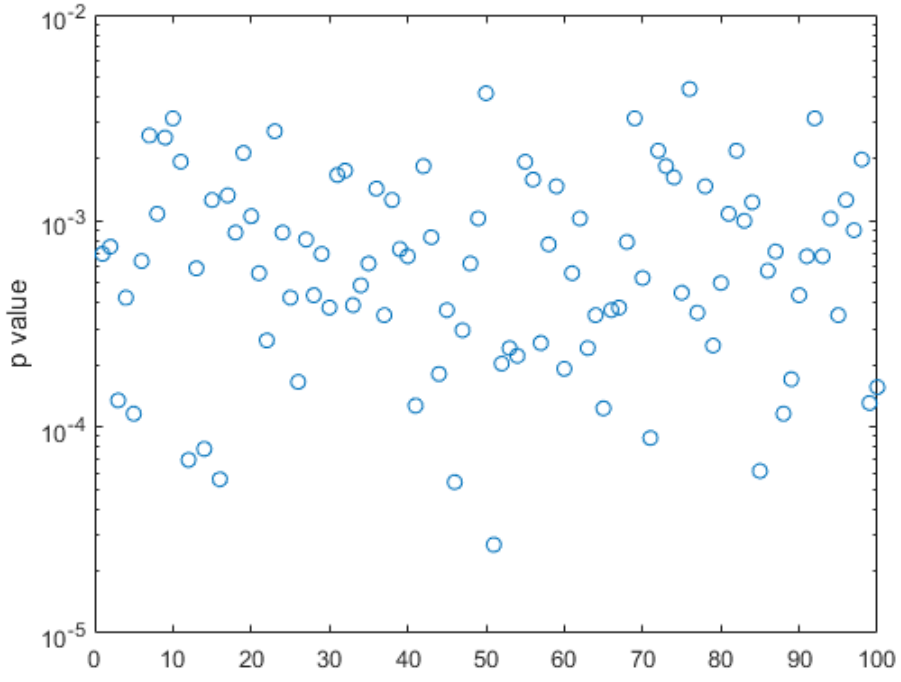

Figure 4.10: Representation of the obtained p values during cross validation between the PoP results obtained for the male control group and the male COPD group. Highest p value obtained: $p_{max} = 4,4 \times 10^{-3}$.

4.4 General Discussion

The obtained results reveal some potential for the GI and the PoP indexes as viable parameters for COPD testing and monitoring.

Both of these parameters present little variance between breathing cycles in the same data set (as demonstrated by the low SDs obtained for all data sets). A low variance was also obtained between different datasets of the same subject. This stability is an important quality: if the parameter had large variance within the same subject, comparing its values between different subjects would be more difficult and would require acquisitions over a large period of time.

It is important to note, however, that while significant differences were obtained between the control and the COPD group, an overlap between the highest values from the control group and the lowest values from the COPD group is present for both parameters. We therefore recommend that these parameters should be used along with other parameters and other ways of diagnosis and monitoring in order to reduce the false positive and false negative rate.

To better understand the classification performance of the studied parameters a receiver operating characteristic (ROC), described in Section 3.5, was computed.

The obtained ROC curves are displayed in Figure 4.11. While the GI and LI indexes had bad performance scores, with an area under curve (AUC) of 0.66 and 0.67 respectively, PoP obtained a strong result with an AUC of 0.82.

Finally, the sample size of the data available for testing is relatively small. To validate the results of this study, and to better understand the strengths and weaknesses of these parameters, further testing needs to be done.

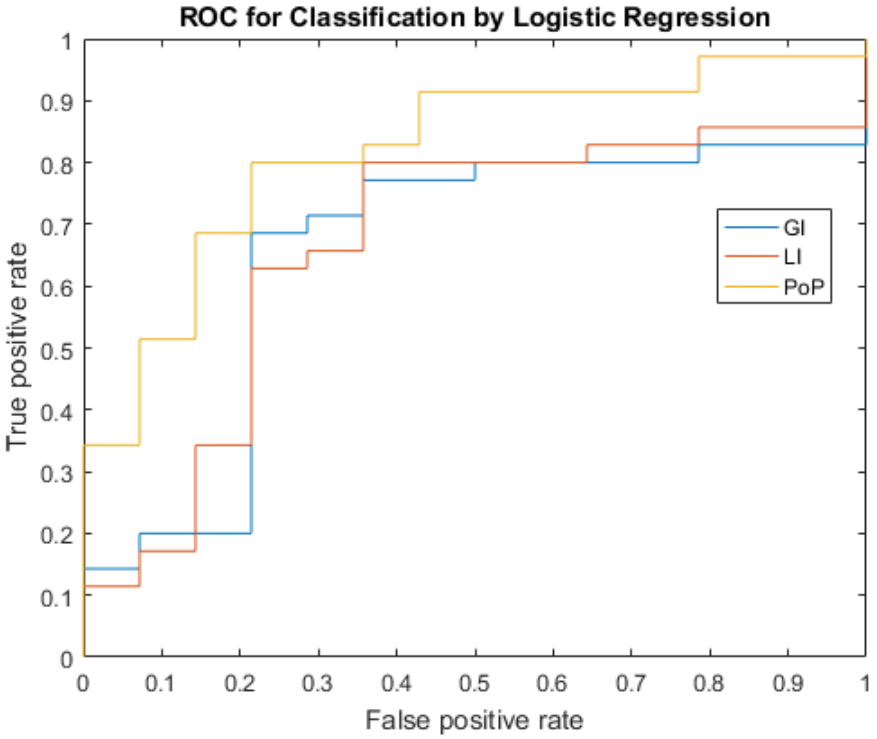

Figure 4.11: ROC for classification by Logistic Regression. AUC values for each curve: $AUC_{GI} = 0.66, AUC_{LI} = 0.67, AUC_{PoP} = 0.82$.

Chapter 5

Conclusion and Future Work

This thesis contribution consists in the implementation and testing of three different parameters that measure lung ventilation heterogeneity. These parameters could see use in devices like the wearable vest that the WELCOME project aims to design and implement whose function would be to provide continuous monitoring of COPD patients.

In order to evaluate the viability of these parameters, the steps followed were:

- Study of the problem and review of relevant literature about EIT monitoring of lung function.
- Reconstruction of EIT images from the datasets, using the GREIT reconstruction algorithm with the help of the EIDORS library for MATLAB. Computation of a tidal image for each breathing cycle.
- Implementation of these parameters. Analysis of the obtained data using the Kruskal-Wallis test and Monte Carlo cross validation and evaluation of the performance of the parameters by computation of the ROC curve.

From the studied parameters PoP had the most promising results. The Kruskal-Wallis test and cross validation returned significant differences between the control and the COPD group. The parameter also exhibited a strong performance in terms of classification. These parameters allow interpatient comparisons, so there is a clear potential for its use in testing and/or monitoring of COPD. The GI index also returned significant differences between the groups. Its classification performance was however far worse than

the one from PoP. Finally, the LI index did not obtain significant differences between the control and the COPD group.

Further testing needs to be done to see these parameters in clinical use. To start, once more data is available, future studies should focus on whether some patients' characteristics like gender, age and body mass influence these parameters and, if the answer is positive, understand exactly how. Furthermore, to make these parameters useful for monitoring of COPD patients over a long period of time, it is necessary to understand how these parameters behave with the progression of the disease.

References

[1] C. J. Murray and A. D. Lopez, "Alternative projections of mortality and disability by cause 1990–2020: Global burden of disease study," *The Lancet*, vol. 349, no. 9064, pp. 1498–1504, 1997.

[2] T. L. Feenstra, M. L. van Genugten, R. T. Hoogenveen, E. F. Wouters, and M. P. Rutten-van Mölken, "The impact of aging and smoking on the future burden of chronic obstructive pulmonary disease: a model analysis in the netherlands," *American journal of respiratory and critical care medicine*, vol. 164, no. 4, pp. 590–596, 2001.

[3] World Health Organization, "The top 10 causes of death," http://who.int/mediacentre/factsheets/fs310/en/, 2004, acessed: 2016-04-12.

[4] S. D. Sullivan, S. D. Ramsey, and T. A. Lee, "The economic burden of copd," *CHEST Journal*, vol. 117, no. 2_suppl, pp. 5S–9S, 2000.

[5] D. M. Mannino and A. S. Buist, "Global burden of copd: risk factors, prevalence, and future trends," *The Lancet*, vol. 370, no. 9589, pp. 765–773, 2007.

[6] M. Ferrer, J. Alonso, J. Morera, R. M. Marrades, A. Khalaf, M. C. Aguar, V. Plaza, L. Prieto, and J. M. Anto, "Chronic obstructive pulmonary disease stage and health-related quality of life," *Annals of internal Medicine*, vol. 127, no. 12, pp. 1072–1079, 1997.

[7] J. Vestbo, S. S. Hurd, A. G. Agustí, P. W. Jones, C. Vogelmeier, A. Anzueto, P. J. Barnes, L. M. Fabbri, F. J. Martinez, M. Nishimura *et al.*, "Global strategy for the diagnosis, management, and prevention of chronic obstructive pulmonary disease: Gold executive summary," *American journal of respiratory and critical care medicine*, vol. 187, no. 4, pp. 347–365, 2013.

[8] T. Schermer, J. Jacobs, N. Chavannes, J. Hartman, H. Folgering, B. Bottema, and C. Van Weel, "Validity of spirometric testing in a general practice population of patients with chronic obstructive pulmonary disease (copd)," *Thorax*, vol. 58, no. 10, pp. 861–866, 2003.

[9] WELCOME - Wearable Sensing and Smart Cloud Computing for Integrated Care to COPD Patients with Comorbidities, "About the project," http://www.welcome-project.eu/about-the-project.aspx, acessed: 2015-12-05.

[10] A. Adler, M. B. Amato, J. H. Arnold, R. Bayford, M. Bodenstein, S. H. Böhm, B. H. Brown, I. Frerichs, O. Stenqvist, N. Weiler *et al.*, "Whither lung eit: Where are we, where do we want to go and what do we need to get there?" *Physiological measurement*, vol. 33, no. 5, p. 679, 2012.

[11] I. Frerichs, T. Becher, and N. Weiler, "Electrical impedance tomography imaging of the cardiopulmonary system," *Current opinion in critical care*, vol. 20, no. 3, pp. 323–332, 2014.

[12] Premed HQ, "Anatomy of the lung and alveoli," https://www.premedhq.com/structure-of-lungs-and-alveoli, 2016, acessed: 2016-08-12.

[13] National Heart, Lung and Blood Institute, "What is copd?" http://www.nhlbi.nih.gov/health/health-topics/topics/copd, 2004, acessed: 2016-01-05.

[14] T. Vos, A. D. Flaxman, M. Naghavi, R. Lozano, C. Michaud, M. Ezzati, K. Shibuya, J. A. Salomon, S. Abdalla, V. Aboyans *et al.*, "Years lived with disability (ylds) for 1160 sequelae of 289 diseases and injuries 1990–2010: a systematic analysis for the global burden of disease study 2010," *The Lancet*, vol. 380, no. 9859, pp. 2163–2196, 2013.

[15] World Health Organization, "Burden of copd," http://www.who.int/respiratory/copd/burden/en/, 2004, acessed: 2015-12-05.

[16] T. Tidswell, A. Gibson, R. H. Bayford, and D. S. Holder, "Three-dimensional electrical impedance tomography of human brain activity," *NeuroImage*, vol. 13, no. 2, pp. 283–294, 2001.

[17] A. P. Bagshaw, A. D. Liston, R. H. Bayford, A. Tizzard, A. P. Gibson, A. T. Tidswell, M. K. Sparkes, H. Dehghani, C. D. Binnie, and D. S. Holder, "Electrical

impedance tomography of human brain function using reconstruction algorithms based on the finite element method," *NeuroImage*, vol. 20, no. 2, pp. 752–764, 2003.

[18] B. Brown, "Electrical impedance tomography (eit): a review," *Journal of medical engineering & technology*, 2009.

[19] A. Adler, B. Grychtol, and R. Bayford, "Why is eit so hard, and what are we doing about it?" *Physiological measurement*, vol. 36, no. 6, p. 1067, 2015.

[20] D. Barber and B. Brown, "Applied potential tomography," *Journal of Physics E: Scientific Instruments*, vol. 17, no. 9, p. 723, 1984.

[21] G. J. Saulnier, R. S. Blue, J. C. Newell, D. Isaacson, and P. M. Edic, "Electrical impedance tomography," *IEEE Signal Processing Magazine*, vol. 18, no. 6, pp. 31–43, 2001.

[22] R. Bayford and A. Tizzard, "Bioimpedance imaging: an overview of potential clinical applications," *Analyst*, vol. 137, no. 20, pp. 4635–4643, 2012.

[23] J. A. Victorino, J. B. Borges, V. N. Okamoto, G. F. Matos, M. R. Tucci, M. P. Caramez, H. Tanaka, F. S. Sipmann, D. C. Santos, C. S. Barbas *et al.*, "Imbalances in regional lung ventilation: a validation study on electrical impedance tomography," *American Journal of Respiratory and Critical Care Medicine*, vol. 169, no. 7, pp. 791–800, 2004.

[24] I. Frerichs, P. A. Dargaville, T. Dudykevych, and P. C. Rimensberger, "Electrical impedance tomography: a method for monitoring regional lung aeration and tidal volume distribution?" *Intensive care medicine*, vol. 29, no. 12, pp. 2312–2316, 2003.

[25] E. L. Costa, C. N. Chaves, S. Gomes, M. A. Beraldo, M. S. Volpe, M. R. Tucci, I. A. Schettino, S. H. Bohm, C. R. Carvalho, H. Tanaka *et al.*, "Real-time detection of pneumothorax using electrical impedance tomography," *Critical care medicine*, vol. 36, no. 4, pp. 1230–1238, 2008.

[26] S. Lindgren, H. Odenstedt, C. Olegård, S. Söndergaard, S. Lundin, and O. Stenqvist, "Regional lung derecruitment after endotracheal suction during volume-or pressure-controlled ventilation: a study using electric impedance tomography," *Intensive care medicine*, vol. 33, no. 1, pp. 172–180, 2007.

[27] T. Meier, H. Luepschen, J. Karsten, T. Leibecke, M. Großherr, H. Gehring, and S. Leonhardt, "Assessment of regional lung recruitment and derecruitment during a peep trial based on electrical impedance tomography," *Intensive care medicine*, vol. 34, no. 3, pp. 543–550, 2008.

[28] A. Adler, N. Shinozuka, Y. Berthiaume, R. Guardo, and J. H. Bates, "Electrical impedance tomography can monitor dynamic hyperinflation in dogs," *Journal of Applied Physiology*, vol. 84, no. 2, pp. 726–732, 1998.

[29] J. A. Frank and M. A. Matthay, "Science review: mechanisms of ventilator-induced injury," *Critical Care*, vol. 7, no. 3, p. 1, 2002.

[30] J.-J. Rouby, L. Puybasset, A. Nieszkowska, and Q. Lu, "Acute respiratory distress syndrome: lessons from computed tomography of the whole lung," *Critical care medicine*, vol. 31, no. 4, pp. S285–S295, 2003.

[31] C. L. Yang, "Electrical impedance tomography: algorithms and applications," Ph.D. dissertation, University of Bath, 2014.

[32] D. S. Holder, *Electrical impedance tomography: methods, history and applications*. CRC Press, 2004.

[33] A. Adler, J. H. Arnold, R. Bayford, A. Borsic, B. Brown, P. Dixon, T. J. Faes, I. Frerichs, H. Gagnon, Y. Gärber *et al.*, "Greit: a unified approach to 2d linear eit reconstruction of lung images," *Physiological measurement*, vol. 30, no. 6, p. S35, 2009.

[34] A. Boyle and A. Adler, "The impact of electrode area, contact impedance and boundary shape on eit images," *Physiological measurement*, vol. 32, no. 7, p. 745, 2011.

[35] A. Adler, P. O. Gaggero, and Y. Maimaitijiang, "Adjacent stimulation and measurement patterns considered harmful," *Physiological measurement*, vol. 32, no. 7, p. 731, 2011.

[36] I. Frerichs, J. Hinz, P. Herrmann, G. Weisser, G. Hahn, T. Dudykevych, M. Quintel, and G. Hellige, "Detection of local lung air content by electrical impedance tomography compared with electron beam ct," *Journal of applied physiology*, vol. 93, no. 2, pp. 660–666, 2002.

[37] G. Hahn, T. Dudykevych, I. Frerichs, F. Thiel, and G. Hellige, "A high performance electrical impedance tomography (eit) system for clinical evaluation studies and space application," in *Proc. Conf. 2nd European Medical and Biological Engineering (Vienna, Austria)*, 2002, pp. 110–1.

[38] E. Teschner, M. Imhoff, and S. Leonhardt, "Electrical impedance tomography: The realization of regional ventilation monitoring," *Dräger Medical GmbH*, 2011.

[39] J.-L. Vincent, *Yearbook of Intensive Care and Emergency Medicine 2009*. Springer Science & Business Media, 2009.

[40] C. H. Antink, R. Pikkemaat, J. Malmivuo, and S. Leonhardt, "A shape-based quality evaluation and reconstruction method for electrical impedance tomography," *Physiological measurement*, vol. 36, no. 6, p. 1161, 2015.

[41] B. Brown and A. Seagar, "The sheffield data collection system," *Clinical Physics and Physiological Measurement*, vol. 8, no. 4A, p. 91, 1987.

[42] W. R. Lionheart, "Eit reconstruction algorithms: pitfalls, challenges and recent developments," *Physiological measurement*, vol. 25, no. 1, p. 125, 2004.

[43] R. Olmi, M. Bini, and S. Priori, "A genetic algorithm approach to image reconstruction in electrical impedance tomography," *IEEE Transactions on Evolutionary Computation*, vol. 4, no. 1, pp. 83–88, 2000.

[44] A. Adler, J. Arnold, R. Bayford, A. Borsic, B. Brown, P. Dixon, T. Faes, I. Frerichs, H. Gagnon, Y. Garber *et al.*, "Greit: towards a consensus eit algorithm for lung images," 2008.

[45] A. Adler and W. R. Lionheart, "Uses and abuses of eidors: an extensible software base for eit," *Physiological measurement*, vol. 27, no. 5, p. S25, 2006.

[46] Z. Zhao, K. Möller, D. Steinmann, and J. Guttmann, "Global and local inhomogeneity indices of lung ventilation based on electrical impedance tomography," in *4th European Conference of the International Federation for Medical and Biological Engineering*. Springer, 2009, pp. 256–259.

[47] Z. Zhao, K. Möller, D. Steinmann, I. Frerichs, and J. Guttmann, "Evaluation of an electrical impedance tomography-based global inhomogeneity index for pulmonary

ventilation distribution," *Intensive care medicine*, vol. 35, no. 11, pp. 1900–1906, 2009.

[48] T. Becher, M. Kott, D. Schädler, B. Vogt, T. Meinel, N. Weiler, and I. Frerichs, "Influence of tidal volume on ventilation inhomogeneity assessed by electrical impedance tomography during controlled mechanical ventilation," *Physiological measurement*, vol. 36, no. 6, p. 1137, 2015.

[49] Z. Zhao, S. Pulletz, I. Frerichs, U. Müller-Lisse, and K. Möller, "The eit-based global inhomogeneity index is highly correlated with regional lung opening in patients with acute respiratory distress syndrome," *BMC research notes*, vol. 7, no. 1, p. 82, 2014.

Appendix A

GREIT figures of merit

This appendix is based on the work of Adler *et al 2009* [33]. The GREIT figures of merit consider an EIT system using the following notation described by the authors:

"Using n_E electrodes, n_E current stimulation patterns are sequentially applied and n_V differential voltage measurements are made in parallel for each stimulation. For an adjacent drive EIT system, voltages are typically not measured at driven electrodes and $n_V = n_E - 3$. Each data frame measures a vector, $v \in \mathbb{R}^{n_M}$, of $n_M = n_E n_V$ data points (some of which are redundant if the medium is not changing). Difference EIT calculates difference data y, ($[y]_i = [v]_i - [v_r]_i$), where v_r is a reference set of measurements corresponding to the background conductivity distribution, σ_r. To improve its precision, v_r is typically averaged over many data frames, such ensemble averaging reduces random noise, and we assume that v_r is noise free."

As explained in Section 2.4 and using the notation described below, given a vector of EIT difference data y, of length $n_E n_V$, it is possible to calculate a reconstructed EIT image $\hat{x} = Ry$ based on an EIT linear reconstruction algorithm represented as a matrix R. $\hat{x}$ is a column vector representing the 32 x 32 pixel grid of the images.

The figures of merit of GREIT are calculated based on small "point" conductivity changes, with a diameter of less than 5% of the medium diameter, so much smaller than the spatial resolution of an EIT device with 16 electrodes.

To evaluate the image, a $\frac{1}{4}$ amplitude set is first calculated, which is represented by this notation as $\hat{x}_q$. This contains all image pixels $[\hat{x}]_i$ greater than $\frac{1}{4}$ of the maximum amplitude:

$$[\hat{x}_q]_i = \begin{cases} 1 & if [x]_i \geq \frac{1}{4} max(\hat{x}) \\ 0 & otherwise \end{cases}$$

The following figures of merit were defined (figure A.1):

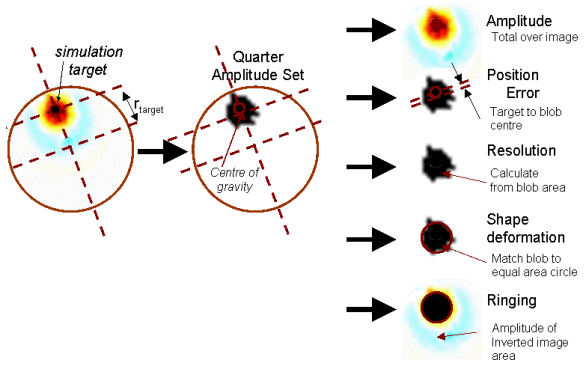

Figure A.1: Performance figures of merit selected for evaluation of GREIT images. Based on a reconstructed image ($\hat{x}$), another image ($\hat{x}_q$) is constructed of all image pixels which exceed $\frac{1}{4}$ the maximum amplitude. From these images figures of merit are calculated. Image extracted from [33].

The figures of merit, in order of importance, are:

- **Uniform amplitude response (AR)**. AR measures the ratio of image pixel amplitudes in the target to that in the reconstructed image. It is defined as: "for a spherical target of volume V_t in the electrode plane with conductivity σ_t in a body of homogeneous reference conductivity σ_r

$$AR = \frac{\sum_k [\hat{x}]_k}{V_t \frac{\Delta\sigma}{\sigma_r}}$$

  where $\Delta\sigma = \sigma_t - \sigma_r$".

  AR should be constant for any target position because without constant amplitude response the same volume of air in different parts of the lung will contribute differently to the image, therefore introducing severe difficulties in image interpretation.

- **Small and uniform Position Error (PE)**. PE measures how close the reconstructed images represent the position of the image target. Based on the target position, r_t, and the CoG of $\hat{x}_q$, r_q, PE is defined by the authors as:

$$PE = r_t - r_q$$

So, PE basically measures how far the center of gravity of the reconstructed resistivity distribution is relatively to the ground truth.

If PE is not uniform, interpretation of a distribution of air in the lungs is unreliable. For example the Sheffield backprojection, one of the first and most widely used reconstruction algorithms, has an higher PE near the electrodes. This lead to cases where changes at the electrodes are misinterpreted as being inside the body.

- **Uniform Resolution (RES)**. RES intends to measure the size of the reconstructed target as a fraction of the medium. This is equivalent to a measure of point spread function (PSF) size. RES is defined as:

$$RES = \sqrt{\frac{A_q}{A_0}}$$

where A_q is the number of pixels in $\hat{x}_q$ and A_0 is the number of pixels in the entire reconstructed medium.

An uniform and small RES allows an accurate representation of the target conductivity distribution. While a non-uniform RES can lead to an incorrect reconstructed position of a larger target, low RES is important for distinguishability in nearby targets.

An uniform RES is considered to be a more important characteristic than a low one. EIT having a low spatial resolution is a known and accepted drawback compared to other medical imaging techniques, due to the limitation on the number of independent measurements by the number of electrodes in the EIT system, so the ability to distinguish nearby targets is considered less important.

- **Limited Shape Deformation (SHD)**. Reconstruction algorithms create circular images for targets in the centre, but often display strangely shaped artefacts for targets near the medium boundary. Adler *et. al* [33] describe SHD as the measure

of "the fraction of the reconstructed $\frac{1}{4}$ amplitude set which does not fit within a circle of equal area.

$$SHD = \frac{\sum\limits_{k \notin C} [\hat{x}_q]_k}{\sum\limits_{k} [\hat{x}_q]_k}$$

where C is a circle at the CoG of $[\hat{x}_q]$ with an equivalent area to A_q."

A large SHD may result in incorrect interpretation of images.

- **Low and uniform Ringing (RNG)**. RNG determines whether reconstructed images show areas of opposite sign surrounding the main reconstructed target area. The function of RNG is to measure "the ratio of image amplitude of the opposite sign outside circle C to image amplitude within C" [33].

$$RNG = \frac{\sum\limits_{k \notin C \& [\hat{x}_q] < 0} [\hat{x}]_k}{\sum\limits_{k \in C} [\hat{x}]_k}$$

Explained in another way, RNG determines how much negative resistivity, that makes no physical sense, is reconstructed.

- **Low Noise Amplification (NF)** measures by how much a random measurement noise is amplified in the reconstructed images. NF is the ratio of the output to input signal to noise ratio (SNR) for a filter (figure A.2). SNR is defined as $SNR = \frac{mean|signal|}{stdnoise}$. So NF is equal to:

$$NF = \frac{E[mean|\hat{x}_t|]/E[std\hat{x}_n]}{E[mean|y_t|]/E[stdy_n]}$$

For GREIT, the value of NF is set by the weighting associated with the training noise. NF should be low but there is an inherent trade-off between good noise performance and fidelity to the other figures of merit. So the ideal value of NF should be around the noise level present in the EIT hardware used. Several studies have been done to select an appropriate value of noise performance without large consensus, but the noise performance of the Sheffield Backprojection algorithm, of $NF = 0.5$ in the medium center, has generally been considered satisfactory, being therefore a recommended value for the GREIT algorithm [33].

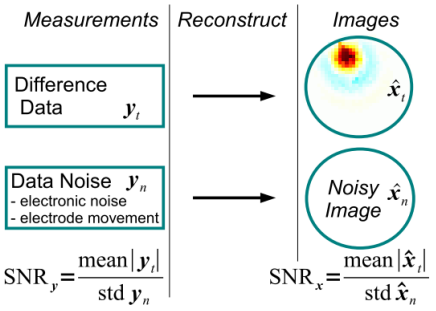

Figure A.2: Schematic representation of the Noise Figure parameter. This parameter represents the amplification of noise through the reconstruction process as the ratio of SNR_x to SNR_y. Image extracted from [33].

Appendix B

Tidal Images Computed

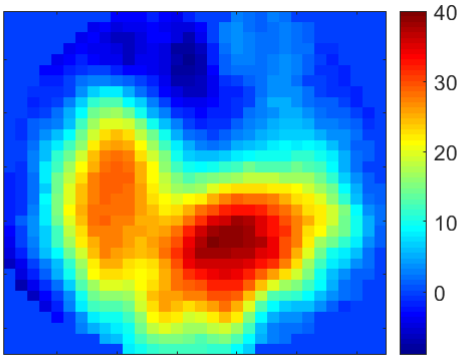

Figure B.1: Tidal image obtained from healthy subject #5.

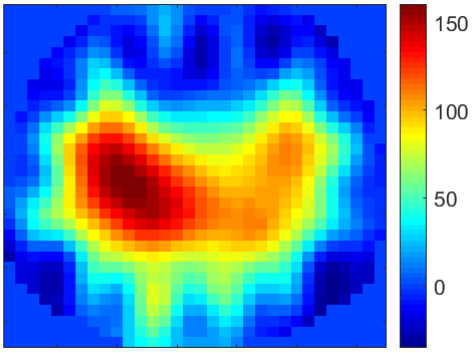

Figure B.2: Tidal image obtained from healthy subject #6.

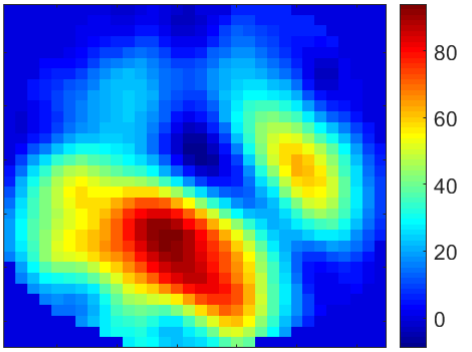

Figure B.3: Tidal image obtained from healthy subject #7.

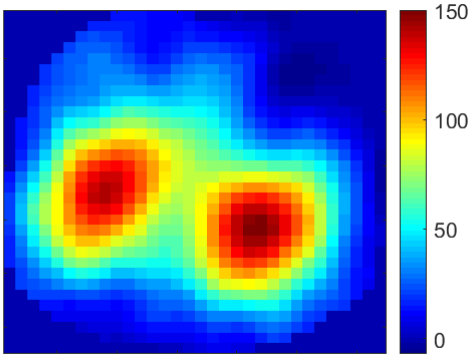

Figure B.4: Tidal image obtained from healthy subject #8.

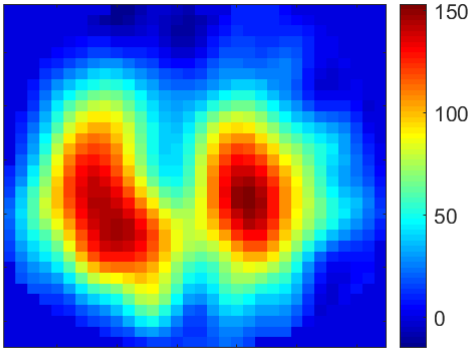

Figure B.5: Tidal image obtained from healthy subject #9.

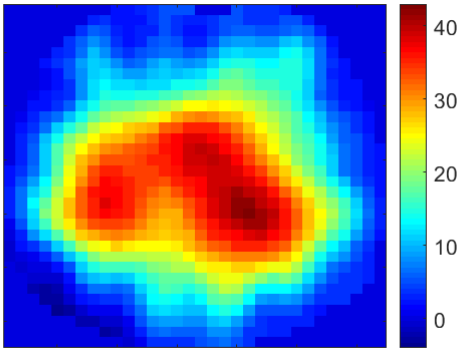

Figure B.6: Tidal image obtained from healthy subject #10.

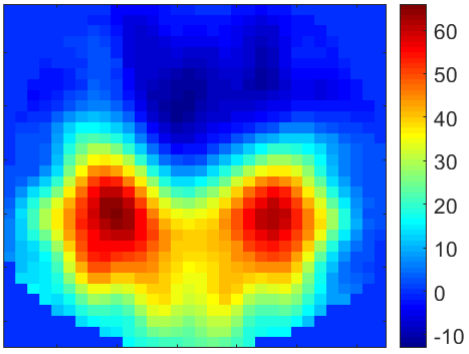

Figure B.7: Tidal image obtained from patient #1.

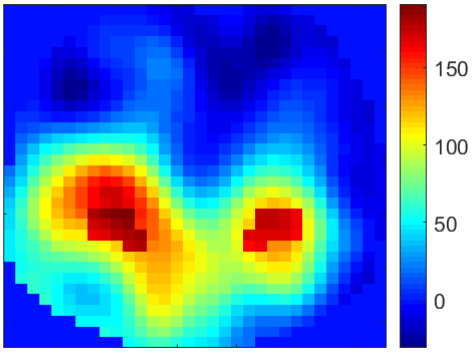

Figure B.8: Tidal image obtained from patient #2.

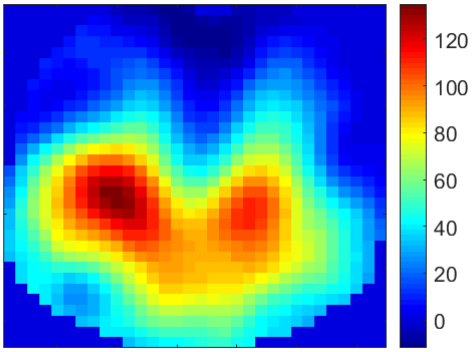

Figure B.9: Tidal image obtained from patient #3.

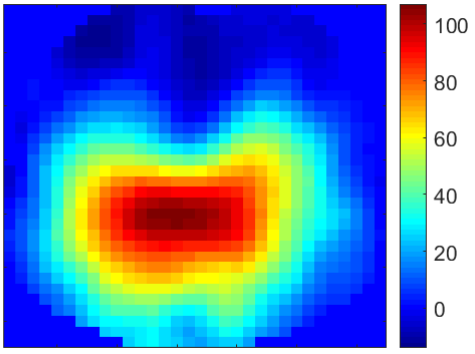

Figure B.10: Tidal image obtained from patient #4.

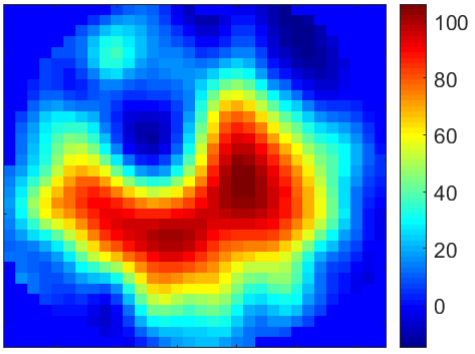

Figure B.11: Tidal image obtained from patient #5.

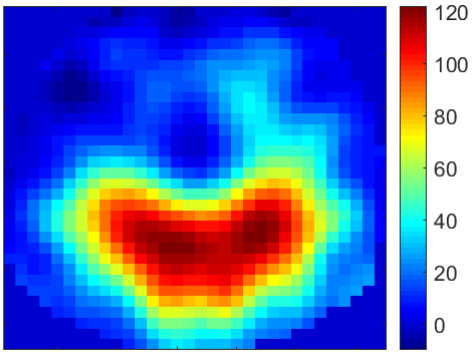

Figure B.12: Tidal image obtained from patient #6.

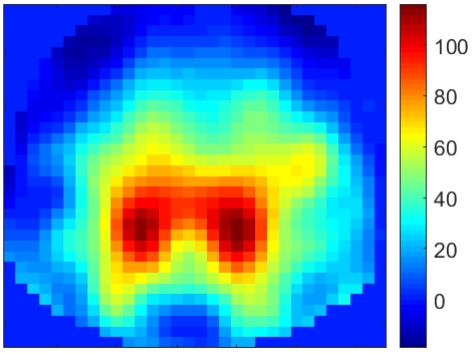

Figure B.13: Tidal image obtained from patient #7.

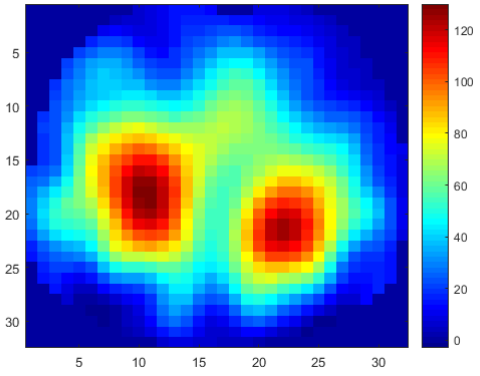

Figure B.14: Tidal image obtained from patient #8.

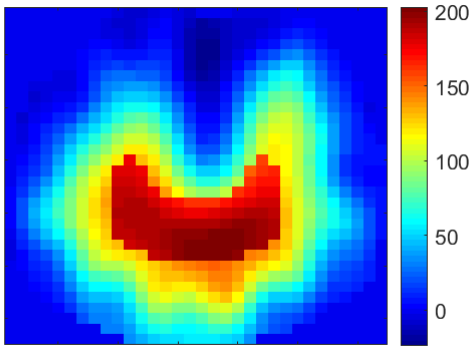

Figure B.15: Tidal image obtained from patient #9.

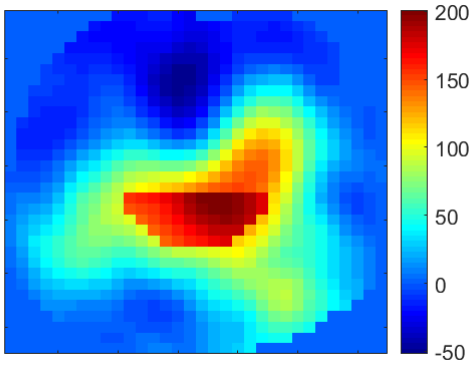

Figure B.16: Tidal image obtained from patient #10.

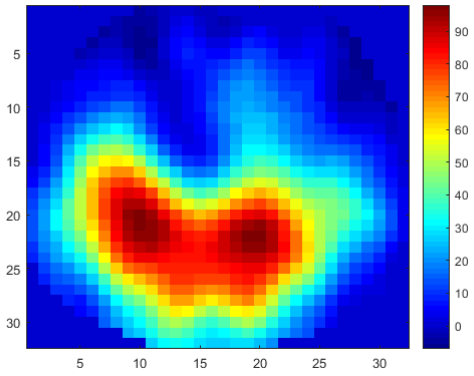

Figure B.17: Tidal image obtained from patient #11.

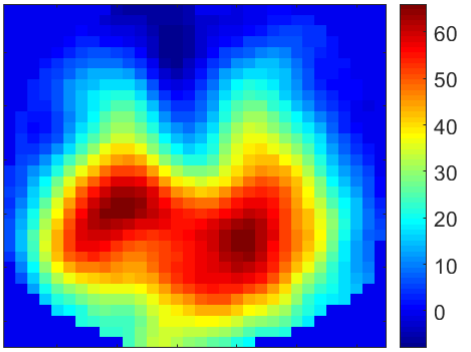

Figure B.18: Tidal image obtained from patient #12.

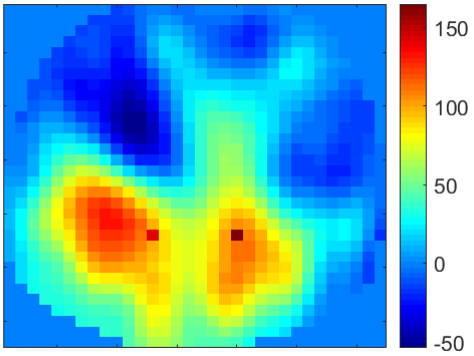

Figure B.19: Tidal image obtained from patient #13.

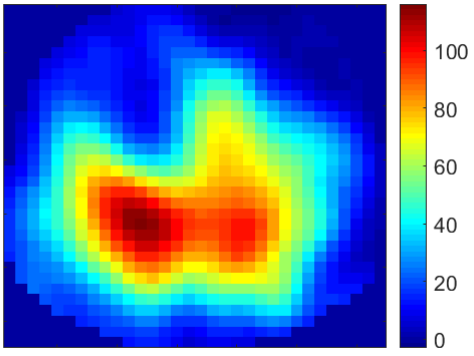

Figure B.20: Tidal image obtained from patient #14.

Appendix C

Proceeding Paper Published

Evaluation of lung ventilation distribution in chronic obstructive pulmonary disease patients using the global inhomogeneity index

F. Trenk[1], L. Mendes[1], P. Carvalho[1], J. Henriques[1]
N. Maglaveras[2], I. Chouvarda[2], V. Tsara[3] and C. A. Teixeira[1]

***Abstract*— The global inhomogeneity (GI) index is a electrical impedance tomography (EIT) parameter that quantifies the tidal volume distribution within the lung. In this work the global inhomogeneity index was computed for twenty subjects in order to evaluate his potential use in the detection and follow up of chronic obstructive pulmonary disease (COPD) patients.**

EIT data of 17 subjects were acquired: 14 patients with the main diagnoses of COPD and 3 healthy subjects which served as a control group. Two or three datasets of around 30 seconds were acquired at 33 scans/s and analysed for each subject. After reconstruction, a tidal EIT image was computed for each breathing cycle and a GI index calculated from it.

Results have shown significant differences in GI values between the two groups (0.745 $\pm$ 0.007 for COPD and 0.668 $\pm$ 0.006 for lung-healthy subject, $p < 0.005$). The GI values obtained for each subject have shown small variance between them, which is a good indication of stability. The results suggested that the GI may be useful for the identification and follow up of ventilation problems in patients with COPD.

I. INTRODUCTION

Pulmonary air flow is less than normal in certain lung areas of chronic obstructive pulmonary disease (COPD) patients. This leads to a higher ventilation inhomogeneity than in healthy subjects. Therefore, parameters that quantify the degree of this inhomogeneity provide useful information about the lung condition.

Several methods are able to detect this inhomogeneity in ventilation in the lung such as computed tomography [1] and the multibreath washout technique [2]. However, these methods are not suitable for continuous monitoring.

Electrical Impedance Tomography (EIT), while having a lower spatial resolution than CT, can provide a non-invasive, radiation-free and continuous image of pulmonary impedance [3]. This is because lung resistivity is around five times higher when compared to most other soft tissues within the thorax, and its value increases and decreases significantly between inspiration and expiration [4]. Furthermore, due to having high temporal resolution, EIT quickly detects changes in lung ventilation. The reliability of EIT for lung ventilation monitoring has already been confirmed by various studies [5]. However, EIT images obtained from different subjects are hard to compare directly without prior calibration, since the resulting image does not display absolute impedance values.

In this paper we aim to evaluate the lung condition of COPD patients by calculating the global inhomogeneity (GI) index, a parameter that quantifies ventilation inhomogeneity with a single number [6]. This parameter is calculated from tidal EIT images that represent differences in impedance between end inspiration and end expiration. The GI index has been used mainly with patients under mechanical ventilation in mind, in particular acute respiratory distress syndrome (ARDS) patients [7][8][9], and has shown to be reliable and interpatient comparable [7]. To the best of our knowledge this is the first work that evaluates the viability of this parameter for COPD patients during tidal breathing.

II. METHODS AND DATA

A. Database

Datasets from 17 adult subjects were examined, each around 30 seconds long. Three healthy subjects (37.7 $\pm$ 4.6 years old, mean age $\pm$ SD; female/male: 1/2) and 14 patients (72.8 $\pm$ 8.3 years old; female/male: 2/12) with diagnosis of COPD were examined using EIT. All data was acquired during tidal breathing.

Sixteen self-adhesive electrodes (Blue Sensor L-00-S, Ambu, Ballerup, Denmark) were attached on the chest circumference in the 5-6th intercostal space and one reference electrode on the abdomen in each studied subject.

Measurements involved application of a current (50 kHz, 5 mA$_{rms}$) between two adjacent electrodes, while the voltage is measured by the rest of the electrodes. This process is repeated for current applied between all the adjacent electrode pairs around the body in a sequential process. The EIT data were acquired using the Goe-MF II EIT device (CareFusion, Höchberg, Germany) at around 33 images/s.

This study was approved by the institutional ethics committee and informed written consent was obtained from each study participant.

B. EIT Reconstruction

Raw EIT images were reconstructed from the EIT data using the GREIT algorithm [10]. Reconstruction was done using the EIDORS software: an adult thorax shaped model with a single plane of 16 electrodes and adjacent stimulation pattern was selected from the model library [11]. Each

This work was supported by the European Union project WELCOME (Grant No. 611223).

[1]Centre for Informatics and Systems, Polo II, University of Coimbra, 3030-290 Coimbra, Portugal. felipevieiratrenk@gmail.com, {lgmendes, carvalho, jh, cteixei}@dei.uc.pt

[2]Laboratory of Medical Informatics, Medical School, Aristotle University of Thessaloniki, Thessaloniki, Greece. nicmag@certh.gr, ioannach@certh.gr

[3]Department of Pulmonology, General Hospital of Thessaloniki 'G. Papanikolaou', Thessaloniki, Greece bpneumonologiki@yahoo.gr

obtained EIT image consists of 32×32 pixels, but only 912 of those are pixels of interest, representing the inside of the thorax. The values on these pixels are equal to the normalised difference between the instantaneous and the average pixel impedance for that data set. End-inspiration and end-expiration moments were identified by analysing the global impedance value evolution over time. This value was obtained by calculating the sum of all pixels for each image. At end-inspiration the lungs are filled with air, increasing the measured resistivity on that region, and the total sum of all pixels reaches a maximum. At end-expiration the opposite occurs (step 3 of Figure 2).

A tidal EIT image, showing the impedance difference between end-inspiration and end-expiration, was calculated for each breathing cycle (Figure 1). The higher the volume of air reaching the area represented by each pixel during inspiration, the higher will the value of impedance difference on that pixel be.

C. GI calculation

For each tidal image, the lung area was identified. The lung areas were estimated using functional EIT with a predefined threshold of 35%, i.e., pixels with values larger than 35% of the maximum value in that image were identified as lung area. Since the lungs are expected to be relatively symmetric, the lung area identified was mirrored from left to right and from right to left and combined by a logical OR operation. The final resulting lung area was used to calculate the GI index.

The median value of the pixels in the identified lung area is calculated. The sum of the absolute difference between the median value and every pixel value is considered to represent the variation in tidal volume distribution in the whole lung region [6]. To make the GI index universal and interpatient comparable, it is normalized to the sum of the impedance values within the lung area:

$$GI = \frac{\sum_{x,y \in lung} |DI_{x,y} - Median(DI_{lung})|}{\sum_{x,y \in lung} DI_{xy}} \quad (1)$$

where $DI_{x,y}$ is the value of the differential impedance for the pixel at x, y in the tidal image and DI_{lung} represents all the pixels considered to be part of the lung area.

D. Statistical analysis

Data analysis was performed using MATLAB 8.3 (The Mathworks, Natick, MA, USA). The obtained results were compared using the Kruskal-Wallis test. A p value <0.05 was considered to reject the null hypothesis "GIs from the control and from the COPD group are drawn from the same distribution". Data are presented as mean and standard deviation (SD). An overview of the methodology can be found on Figure 2.

III. RESULTS

Table I shows: the mean GI and number of breathing cycles analysed for each subject and the total weighted mean for each group.

TABLE I

MEAN OF THE GI VALUES OBTAINED FOR EACH OF THE THREE SUBJECTS OF THE CONTROL GROUP AND THE 14 PATIENTS.

Group	GI values (mean ± SD)	# of breathing cycles analyzed
Control Group	0.664 ± 0.009	21
	0.677 ± 0.010	17
	0.661 ± 0.016	19
	Weighted average 0.668 ± 0.006	
COPD Group	0.977 ± 0.035	30
	0.843 ± 0.033	20
	0.660 ± 0.034	19
	0.907 ± 0.041	14
	0.748 ± 0.027	16
	0.732 ± 0.018	22
	0.740 ± 0.022	17
	0.558 ± 0.027	20
	0.795 ± 0.025	27
	1.176 ± 0.049	29
	0.818 ± 0.040	36
	0.581 ± 0.024	31
	1.048 ± 0.037	35
	0.677 ± 0.017	27
	Weighted average 0.745 ± 0.007	

A consistently lower GI value was obtained for the control group (0.668 ± 0.006) compared to the COPD group (0.745 ± 0.007). The standard deviation for the GI index for each subject is relatively small (SD average of 0.012 for control group and 0.030 for COPD patients), which indicates there is little variance between different data sets of each patient.

The GI values obtained for the COPD patients were compared to the control group using the Krustal-Wallis test. The returned p value ($p = 2.10 \times 10^{-11}$) is lower than the significance level, thus rejecting the null hypothesis. Figure 3 compares the obtained GI values for those two groups.

There are significantly more subjects for our COPD group than for the control group. Due to the existence of unbalanced groups, a cross validation was done, by selecting 100 times 57 random GI values from the COPD group and comparing them with the 57 GI values from the control group using the Kruskal-Wallis test. The 100 p values obtained are represented in Figure 4, with all of them being lower than the significance level. These results support the conclusion that there is a consistent difference between the GI values obtained from the COPD group and the control group.

A comparison between the COPD group and the control group for each gender was done as well. There is an high difference between the number of breathing cycles acquired, so a cross validation was done also for gender. The highest p value obtained for both cross validations was lower than the significance level (female $p_{max} = 2.79 \times 10^{-4}$; male $p_{max} = 0.013$). The obtained results are represented at Figure 5 and 6.

IV. DISCUSSION

The method used to define the lung area, while being simple and achieving reasonable results, may contain some pixels related to cardiac activity which may affect the value obtained for the GI parameter [7]. Some methods, like

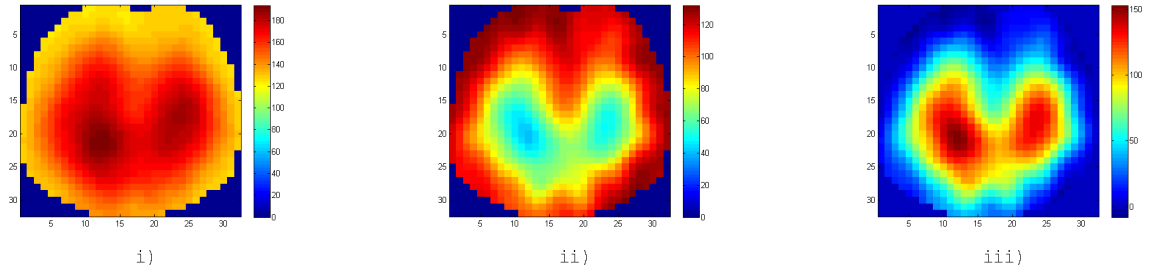

Fig. 1. Image obtained for: i) reconstruction at end-inspiration; ii) reconstruction at end-expiration; iii) the resulting tidal image, equal to the relative impedance difference between the two prior reconstructed images.

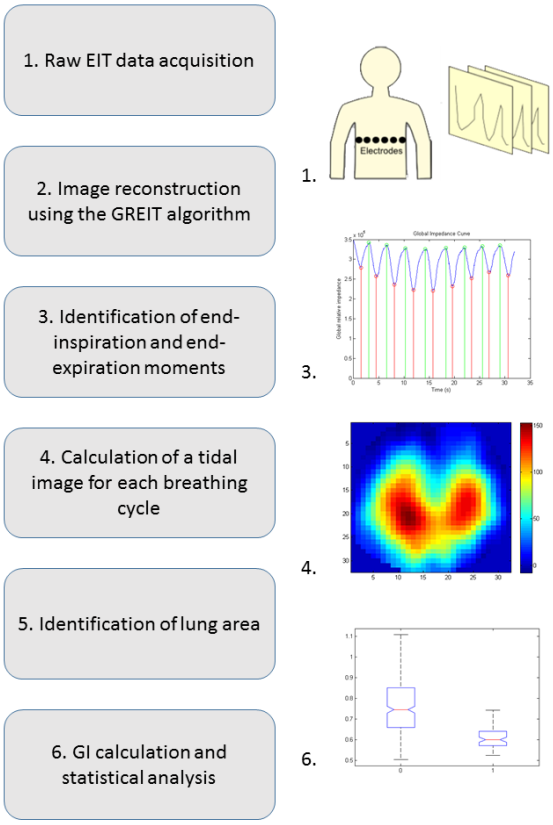

Fig. 2. Diagram of the methodological steps followed for GI calculation.

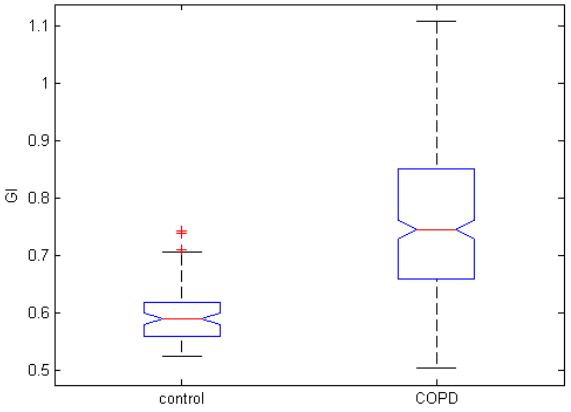

Fig. 3. Comparison of the GI values for the COPD patients and the control group. The boxes represent the quartiles while the whiskers extend from the box out to the most extreme data value within 1.5x the interquartile range of the sample. The red crosses represent outliers.

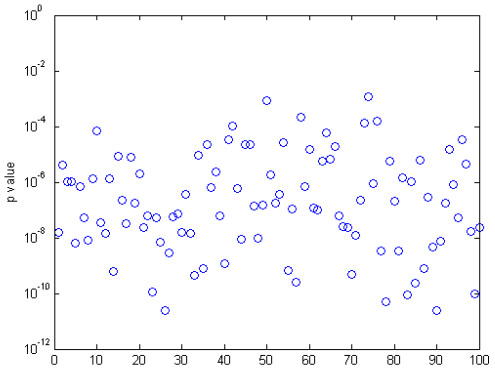

Fig. 4. Representation of the obtained p values during cross validation. Highest p value obtained: 0.0011.

the Lung Area Estimation (LAE) [12] subtract the cardiac related area from the lung area by analysing the energy distribution of every pixel of the tidal EIT image in frequency domain. Cardiac related pixels should have peaks at an higher frequency than lung related pixels.

An important aspect to keep in mind is that the value obtained for the GI index depends on the threshold value used. Higher threshold values in the fEIT method lead to smaller lung area sizes, which lead to different GI values [7]. To keep the GI values interpatient comparable, the chosen threshold value on this study is the same for all subjects of both the COPD patients group and the control group. Another limitation of the GI index is that it only gives a global view

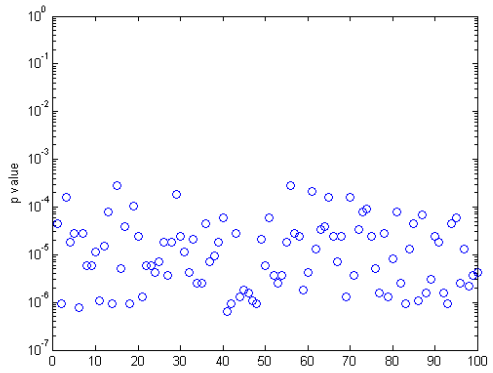

Fig. 5. Representation of the obtained p values during cross validation between female patients and our female control group. Highest p value obtained: $2.79\times\ 10^{-4}$.

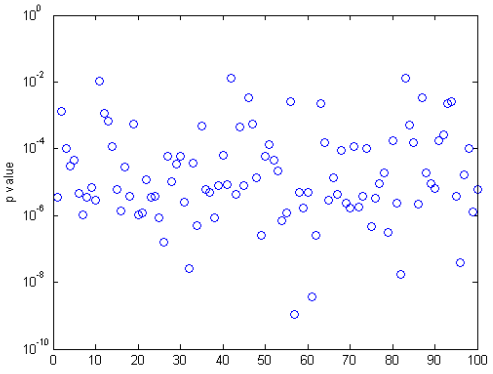

Fig. 6. Representation of the obtained p values during cross validation between male patients and our male control group. Highest p value obtained: 0.013.

of lung ventilation distribution, not considering the local inhomogeneity. We therefore recommend that it should be tested and used with other parameters that emphasize in inhomogeneity on a local level, like the local inhomogeneity (LI) index [6], which quantifies differences among neighbour pixels.

Due to the small sample size available the authors emphasize that the results of this study must be validated with more data.

V. CONCLUSIONS

The GI index is a reliable measure of ventilation heterogeneity. Results have shown significant differences in GI values between COPD patients and the control group. Since the GI index enables interpatient comparison it has great potential. The results suggest that the GI may have potential to be part of a group of parameters that identify and follow the condition of COPD patients under spontaneous respiration.

The control group and the COPD group in this study have high age differences. Future work should test if age by itself is a factor that influences the GI index.

ACKNOWLEDGMENT

We thank all examined patients and healthy subjects for participating in the study. This study was supported by the European Union 7th Framework Programme on R&D (WELCOME project, grant No. 611223).

REFERENCES

[1] L. Gattinoni, P. Caironi, F. Valenza, and E. Carlesso, "The role of ct-scan studies for the diagnosis and therapy of acute respiratory distress syndrome," *Clinics in chest medicine*, vol. 27, no. 4, pp. 559–570, 2006.

[2] A. Schibler and R. Henning, "Positive end-expiratory pressure and ventilation inhomogeneity in mechanically ventilated children," *Pediatric Critical Care Medicine*, vol. 3, no. 2, pp. 124–128, 2002.

[3] A. Adler, M. B. Amato, J. H. Arnold, R. Bayford, M. Bodenstein, S. H. Böhm, B. H. Brown, I. Frerichs, O. Stenqvist, N. Weiler *et al.*, "Whither lung eit: Where are we, where do we want to go and what do we need to get there?" *Physiological measurement*, vol. 33, no. 5, p. 679, 2012.

[4] B. Brown, "Electrical impedance tomography (eit): a review," *Journal of medical engineering & technology*, 2009.

[5] I. Frerichs, T. Becher, and N. Weiler, "Electrical impedance tomography imaging of the cardiopulmonary system," *Current opinion in critical care*, vol. 20, no. 3, pp. 323–332, 2014.

[6] Z. Zhao, K. Möller, D. Steinmann, and J. Guttmann, "Global and local inhomogeneity indices of lung ventilation based on electrical impedance tomography," in *4th European Conference of the International Federation for Medical and Biological Engineering*. Springer, 2009, pp. 256–259.

[7] Z. Zhao, K. Möller, D. Steinmann, I. Frerichs, and J. Guttmann, "Evaluation of an electrical impedance tomography-based global inhomogeneity index for pulmonary ventilation distribution," *Intensive care medicine*, vol. 35, no. 11, pp. 1900–1906, 2009.

[8] T. Becher, M. Kott, D. Schädler, B. Vogt, T. Meinel, N. Weiler, and I. Frerichs, "Influence of tidal volume on ventilation inhomogeneity assessed by electrical impedance tomography during controlled mechanical ventilation," *Physiological measurement*, vol. 36, no. 6, p. 1137, 2015.

[9] Z. Zhao, S. Pulletz, I. Frerichs, U. Müller-Lisse, and K. Möller, "The eit-based global inhomogeneity index is highly correlated with regional lung opening in patients with acute respiratory distress syndrome," *BMC research notes*, vol. 7, no. 1, p. 82, 2014.

[10] A. Adler, J. H. Arnold, R. Bayford, A. Borsic, B. Brown, P. Dixon, T. J. Faes, I. Frerichs, H. Gagnon, Y. Gärber *et al.*, "Greit: a unified approach to 2d linear eit reconstruction of lung images," *Physiological measurement*, vol. 30, no. 6, p. S35, 2009.

[11] A. Adler and W. R. Lionheart, "Uses and abuses of eidors: an extensible software base for eit," *Physiological measurement*, vol. 27, no. 5, p. S25, 2006.

[12] Z. Zhao, K. Möller, D. Steinmann, and J. Guttmann, "Determination of lung area in eit images," in *Bioinformatics and Biomedical Engineering, 2009. ICBBE 2009. 3rd International Conference on*. IEEE, 2009, pp. 1–4.